



POLITECNICO  
DI TORINO



POLITECNICO DI TORINO

MSc. Nanotechnologies for ICTs

DEPARTMENT OF ELECTRONICS AND  
TELECOMMUNICATIONS

---

**Thin and soft hydrogel-coated intracortical probe:  
microfabrication and *in vivo* biointegration**

---

*Candidate*

Valentina Marie Paggi

Matr. 240162

*External supervisors*

Prof. Stéphanie Lacour

Dr. Jennifer Macron

*University supervisors*

Prof. Andrea Lamberti

Prof. Stefano Bianco

Laboratory for Soft Bioelectronic Interfaces  
École Polytechnique Fédérale de Lausanne, Switzerland

Academic year 2017-2018

## Abstract

Intracortical probes are a type of neural interface which can be implanted in the cerebral cortex and offer a high-resolution approach to the stimulation and recording of neural activity. Despite the diagnostic and therapeutic potential of these devices, their clinical applications remain limited due to their performance degradation over time. Recently, a number of studies have been conducted to better understand the mechanisms behind neural implant failure. The onset of an adverse foreign body reaction at the implant-tissue interface is generally associated with the mechanical mismatch between stiff and static devices and soft and dynamic brain tissue. It has been suggested that implanting probes with a minimized cross-section or fabricated with soft, compliant materials can significantly limit neuroinflammation and scarring both over the short and long term.

In this work, these two strategies are combined to fabricate a thin and soft intracortical probe. The proposed device consists of a 10  $\mu\text{m}$  thick flexible polyimide (PI) substrate encapsulated between two layers of poly(2-hydroxyethyl methacrylate) (PHEMA) hydrogel (20  $\mu\text{m}$  on each side). The hydrogel was used to provide mechanical support during insertion and to shield neural tissue from the underlying stiff substrate, after implantation. The mechanical behavior of the multilayered structure was analyzed to assess the conformability and adhesion of the chosen materials, as well as their insertion mechanics. Hydrogel-coated probes were fabricated and tested *in vivo*, and acute tissue response was evaluated. Furthermore, a method was proposed for the development of recording probes, integrating the hydrogel in a standard microfabrication process.

Experiments confirmed a durable integration of polyimide and the hydrogel, which could generate a stiff system to promote insertion and, simultaneously, exhibit a conformability comparable to that of elastomeric materials. Histology results showed minimal tissue damage after 7 days, compared to stiff substrates. Finally, optimization of microfabrication processes, carried out in a dry state to preserve the integrity of the hydrogel, ultimately led to the development of active probes, which have the potential to detect neural activity.

Overall, the obtained results suggest, in a preliminary manner, that it is feasible to develop a hydrogel-coated polyimide probe, which could improve implant biocompatibility, and to incorporate metal electrodes in the proposed thin, soft and flexible system, to provide stable neural sensing and stimulation.

## Sommario

Gli impianti intracorticali sono un tipo di interfaccia neurale in grado di penetrare nella corteccia cerebrale e offrire stimolazione e monitoraggio dell'attività neurale ad alta risoluzione. Nonostante il significativo potenziale diagnostico e terapeutico di tali dispositivi, la loro implementazione clinica è tuttora limitata dal progressivo deterioramento degli impianti stessi. Recentemente, numerosi studi sono stati condotti per identificare i meccanismi responsabili del fallimento di tali dispositivi. L'insorgenza di un'avversa reazione da corpo estraneo all'interfaccia tessuto-impianto è generalmente associata ad una notevole discrepanza tra le proprietà meccaniche dei dispositivi impiantabili rigidi e statici e il tessuto cerebrale morbido e dinamico. Attualmente, si ritiene che l'inserimento di dispositivi con una sezione geometrica ridotta oppure fabbricati con materiali conformabili e morbidi possa ridurre in maniera significativa l'infiammazione e cicatrizzazione del tessuto nervoso sia a breve che a lungo termine.

In questo lavoro, le due strategie sopramenzionate sono state combinate per fabbricare un impianto intracorticale morbido e sottile. Il dispositivo proposto consiste in un substrato flessibile di poliimmide (PI), di spessore  $10\ \mu\text{m}$ , racchiuso tra due strati di poli(2-idrossietil metacrilato) (PHEMA), un idrogel con spessore  $20\ \mu\text{m}$ . L'idrogel è stato utilizzato per fornire un supporto meccanico al dispositivo durante la fase di impiantazione e, in un secondo momento, per agire da strato cuscinetto tra il tessuto nervoso e il substrato più rigido. Il comportamento meccanico del sistema multistrato è stato analizzato per verificarne la conformabilità, valutare l'adesione tra i materiali scelti e per comprendere il meccanismo di inserimento. Gli impianti rivestiti di idrogel sono stati fabbricati e testati *in vivo*, per analizzare la risposta tissutale acuta. Inoltre, è stato proposto un metodo per lo sviluppo di impianti con elettrodi, integrando l'idrogel in un processo standard di microfabbricazione.

Gli esperimenti svolti hanno confermato un'integrazione duratura del complesso idrogel-poliimmide, generando un sistema in grado di promuovere la penetrazione nella corteccia e, al contempo, dotato di una conformabilità paragonabile a quella di elastomeri. L'analisi istologica ha evidenziato la presenza di una ridotta lesione tissutale rispetto a substrati rigidi, dopo 7 giorni. Infine, tramite l'ottimizzazione di processi di microfabbricazione, è stato possibile preservare l'integrità dell'idrogel, mantenendolo sempre in uno stato disidratato, e fabbricare elettrodi impiantabili, potenzialmente in grado di rilevare attività neurale.

Nel complesso i risultati ottenuti suggeriscono, in maniera preliminare, la realizzabilità di un impianto intracorticale di poliimmide racchiuso in idrogel. Tale dispositivo sarebbe in grado di favorire la biointegrazione e di incorporare elettrodi metallici in un sistema sottile, morbido e flessibile, per garantire stimolazione e monitoraggio neurale stabili e a lungo termine.

## **Confidentiality**

The following Master thesis contains confidential data and methods developed at the Laboratory for Soft Bioelectronic Interfaces (LSBI) of the École Polytechnique Fédérale de Lausanne (EPFL, Switzerland). Prior to the publication in scientific research journals, the content of this work shall only be made available to authorized reviewers and examiners. The publication or distribution of this manuscript, in whole or in part, is not permitted for 3 years from the date of submission, unless explicitly authorized by the author and LSBI supervisors.

# Contents

<b>1</b>	<b>Introduction</b>	<b>1</b>
<b>2</b>	<b>State of the art: current perspectives on intracortical probes</b>	<b>4</b>
2.1	Substrate materials . . . . .	4
2.2	Hydrogel/Polymer coatings . . . . .	6
<b>3</b>	<b>Materials and methods</b>	<b>8</b>
3.1	PHEMA hydrogel preparation . . . . .	8
3.2	Material study and integration for passive probes . . . . .	8
3.2.1	Conformability study . . . . .	8
3.2.2	Material integration: surface treatments . . . . .	10
3.2.3	Probe design . . . . .	12
3.2.4	Theoretical model and simulation . . . . .	13
3.2.5	Fabrication method . . . . .	15
3.2.6	<i>In vivo</i> surgery . . . . .	16
3.2.7	Tissue processing and immunohistochemistry . . . . .	17
3.3	Design and fabrication of electroactive probes . . . . .	18
3.3.1	Probe design . . . . .	18
3.3.2	Fabrication method . . . . .	19
3.3.3	Preliminary <i>in vitro</i> and <i>in vivo</i> tests . . . . .	22
<b>4</b>	<b>Results</b>	<b>24</b>
4.1	Passive probes . . . . .	24
4.1.1	Conformability study . . . . .	24
4.1.2	Surface treatments . . . . .	25
4.1.3	Buckling simulation . . . . .	27
4.1.4	Passive probe fabrication . . . . .	29
4.1.5	<i>In vivo</i> study results . . . . .	29
4.2	Electroactive probes . . . . .	32
4.2.1	Probe fabrication and characterization . . . . .	32
4.2.2	Preliminary <i>in vitro</i> and <i>in vivo</i> results . . . . .	36
<b>5</b>	<b>Discussion</b>	<b>37</b>
<b>6</b>	<b>Conclusions</b>	<b>41</b>
6.1	Outlook . . . . .	41
	<b>List of Figures</b>	<b>42</b>
	<b>List of Tables</b>	<b>42</b>
	<b>References</b>	<b>43</b>
	<b>Acknowledgements</b>	<b>48</b>

# 1 Introduction

Neural interfaces are devices designed to establish a direct connection between the nervous system (central and peripheral) and the external world. These devices can either record neural activity, allowing the investigation of the complexity of the nervous system, or stimulate neurons through electrical, chemical or optical mechanisms [1].

They thus act as a versatile tool which shows great promise when used as neuroprosthesis, restoring lost neural functions. Successful applications of such interfaces have already been demonstrated in the treatment of patients with neurological disorders and sensory impairment. Notable examples include cochlear implants, which partially restore hearing by stimulating the auditory nerve [2], devices for deep brain stimulation (DBS), used in the therapeutic treatment of disorders such as essential tremor and Parkinson's disease [3], and visual prostheses for the restoration of sight [4].

Specific subsets of these devices can be applied directly to the central nervous system (CNS) and are commonly referred to as Brain Computer Interfaces (BCI) or Brain Machine Interfaces (BMI) [5]. Breakthroughs in neurotechnology have allowed the development of BCIs which can potentially aid patients with motor dysfunctions, paralysis and limb loss: these interfaces directly extract voluntary control signals generated by neurons in the motor cortex in order to guide an external object, such as a limb prosthesis [6, 7]. Based on its specific application, the neural interface requires a certain level of resolution, which in turn is strictly linked to its invasiveness [5]. For instance, the most commonly used interface in clinical applications is electroencephalography (EEG), a non invasive recording method based on the use of macro-electrodes placed across the entire scalp [8]. It is a simple yet powerful technology which can monitor brain wave activity across broad regions of the brain. Nevertheless, its noninvasiveness inevitably limits the spatial resolution and leads to signal attenuation. As a consequence, its application as BCI is confined to simple devices, mainly for communication (text and speech) [9] or for basic control of external devices, such as wheelchairs [10].

These limitations are overcome by more invasive methods which require a surgical procedure to position electrodes either in direct contact with the surface of the cortex or intracortically/subcortically. The former, known as electrocorticography (ECoG) has found clinical applications in the treatment of epilepsy patients [11], while the latter, implantable electrodes (intracortical probes or deep penetrating probes), have been successfully used for DBS [12]. These implantable electrodes clearly offer the best spatiotemporal resolution, allowing stimulation and recording of specific areas of the brain, and selectivity, by detecting single-neuron activity [13].

Commercially available intracortical probes (e.g. NeuroNexus Michigan probes, Blackrock Microsystems Utah arrays) and those proposed in academic research exist in different geometries and formats, namely microwires, single or multiple shank probes and probe arrays. Normally each shank can incorporate tens of active recording sites, a number which is limited by the width and length of the shank itself. In recent years, however, different groups have worked on the development of high density neural probes, by integrating CMOS circuitry on probe, leading to a more accurate investigation of complex neural activity [14].

While silicon-based devices present clear advantages such as active circuitry integration and a simple, well-established fabrication process, their performance over time tends to degrade. Corrosion of the device due to the biological medium, electrochemical instability of electrode materials (e.g. Pt, IrOx, Au) and structural integrity of the probe play a key role in recording and stimulation degradation and have been extensively analyzed

[15, 16], however they are not to be considered solely responsible. The progressive failure of the implants is also related to the mechanical properties of the probes, in fact it is a common issue of all high Young's modulus materials typically used to fabricate intracortical electrodes (e.g. silicon, steel, tungsten). The mechanical mismatch between soft neural tissue and stiff implants is critical over both the short and long term, causing adverse foreign body reaction (FBR) [17]. The modulus of traditional rigid materials is in the order of few hundred GPa, while tissue in the central nervous system has been quantified to be in the order of hundreds of Pa to few kPa (fig. 1.1). Implanting man-made probes causes mechanical and biological insertion trauma, due to vessel and tissue rupture.

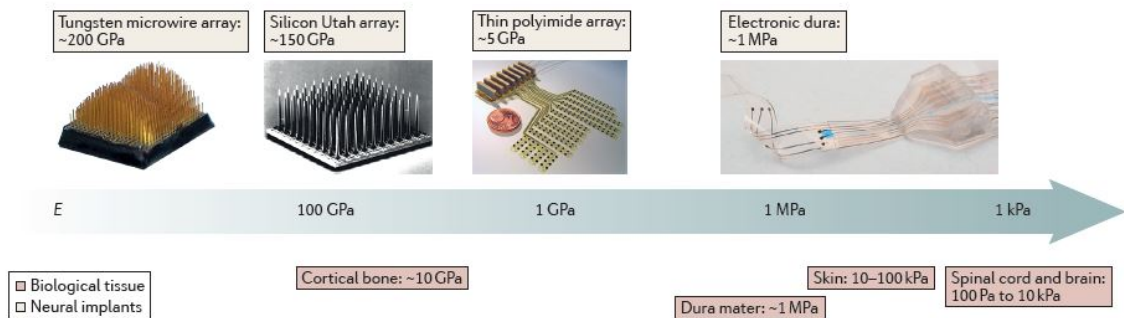


Figure 1.1 – **Mechanical mismatch between stiff implants and soft tissue** [17]. Common implantable electrodes are made of stiff materials such as tungsten and silicon. Recent devices have been fabricated using flexible polymers or elastomers in an attempt to match properties of neural tissue.

In the acute phase of implantation (1-2 weeks) there is an increase in microglia response, which promotes inflammation and can cause a decrease in neuron density around the implant [18]. In the chronic phase (over 4 weeks) there is an observable broadening of glial scar, which isolates the probe from surrounding tissue and leads to an increase in electrode impedance [19], causing issues in both recording and stimulation. A major factor contributing to the formation of glial scar is the presence of micro-motion effects, which become more relevant when a significant mechanical mismatch exists: the brain is subject to constant micro-motion (in the order of few to tens of microns) due to vascular pulsatility and respiratory pressure, which induces strain in soft tissue surrounding the stiff implant, ultimately leading to scar formation [20].

It has been suggested that tissue response can be reduced by matching the mechanical properties of the device to those of the neural tissue and *in vivo* tests have confirmed the beneficial effect of employing more compliant probes (fig 1.2), reporting a reduction in neuronal loss, blood-brain barrier breach, inflammation and scarring around the implantation site [21]. Another crucial factor which can be altered in order to reduce tissue response is device geometry: it has been shown [22] that implants with a smaller cross-section do in fact determine reduced tissue damage during insertion, limiting the possibility of rupturing neighboring vessels. Consequently, the main strategies adopted when designing an intracortical probe consist in employing low modulus materials as main substrate or as soft coating, while trying to reduce the overall footprint of the device.

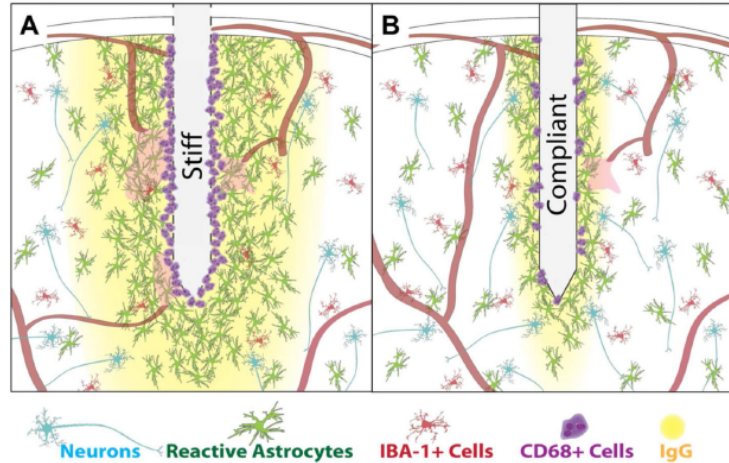


Figure 1.2 – **Schematic comparison of tissue response around stiff (A) and compliant (B) probes** [21]. Stiff implants determine a more significant neuronal loss, glial scar formation, inflammation and permeation of blood-brain barrier.

Research at the Laboratory for Soft Bioelectronic Interfaces (LSBI, EPFL) has focused on achieving precisely these goals for a variety of neural interfaces. The expertise of the group is related to shaping typically rigid devices into more compliant and biocompatible systems, using materials such as polydimethylsiloxane (PDMS) and polyimide (PI). In recent years, work has been conducted to combine these substrates with novel coating materials, with the ultimate goal of producing a fully functional soft device, prepared through standard microfabrication techniques. While the conceived implant should be compliant *in vivo*, a certain degree of rigidity is required to ensure insertion, making mechanically-adaptive materials, such as hydrogels, the ideal coating candidate. In this project the design and fabrication of a hybrid hydrogel-polyimide intracortical probe, which is both thin and soft, is proposed. Its insertion mechanism, its efficacy in reducing tissue inflammation and its potential ability to record neural signals are tested *in vivo*.

The work is organized as follows:

- Chapter 2 proposes a brief overview on the current state of the art for the fabrication of softer, more compliant probes.
- Chapter 3 presents the methods employed to design and fabricate both passive and active probes, as well as their *in vivo* testing.
- Chapter 4 details the main results in terms of material integration, device fabrication and tissue histological analysis.
- Chapter 5 proposes a discussion on obtained results and analyzes the main problematics encountered.
- Finally Chapter 6 reports on the outcome and future developments of the project.

## 2 State of the art: current perspectives on intracortical probes

### 2.1 Substrate materials

A straightforward solution towards reducing foreign body reaction consists in using compliant materials to fabricate implants. Advances in polymeric microfabrication have allowed the substitution of standard microelectronic materials such as tungsten and silicon with polymeric materials with a lower Young's modulus, in the order of a few GPa in the case of flexible substrates, or MPa in the case of elastomers.

#### Flexible substrates

Parylene is among the most popular choices for main substrate material [23–25], due to a variety of advantageous key features. It has high biocompatibility (ISO 10993 USP Class VI material) and a Young's modulus of 2-4 GPa, two orders of magnitude lower than silicon [26]. Parylene can be deposited on a carrier Si wafer through Chemical Vapor Deposition (CVD), a typical microfabrication process. This also makes it possible to integrate metal electrodes (e.g. Pt, Au) through standard techniques. Castagnola *et al.* [24] fabricated flexible parylene-based neural probes with Au electrodes (fig.2.1), reporting successful recording of electrophysiological signals. However, studies have also demonstrated a low adhesion of parylene to materials such as gold and platinum [25], a crucial drawback which could determine device failure.

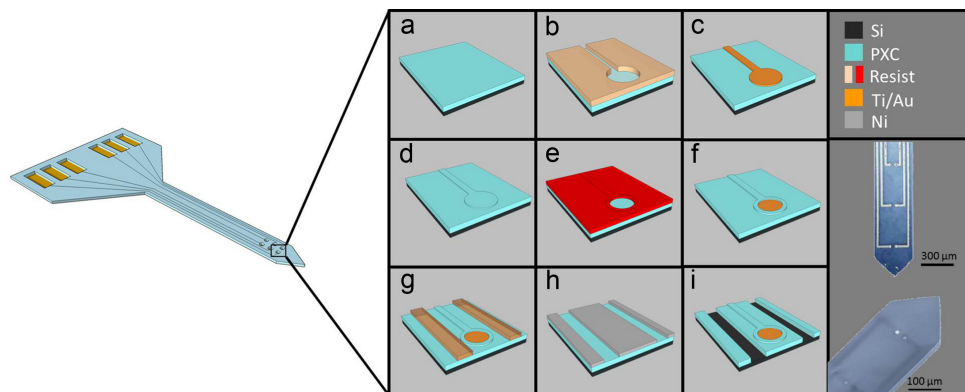


Figure 2.1 – **Schematic illustration of fabrication steps for parylene neural probes** [24]. (a) CVD of parylene, (b) negative resist patterning, (c) Ti/Au e-beam physical vapor deposition and lift off, (d) CVD of parylene, (e) photoresist patterning, (f) dry etching of parylene for contact opening, (g) photoresist patterning, (h) Ni (hard mask) deposition and lift off, (i) dry etching of parylene for release.

Recently parylene probes have been tested *in vivo* to evaluate the glial response [27] from 72 hours up to 24 weeks showing overall improved biocompatibility, which is, however, also significantly contingent on probe dimensions.

Polyimide is another prominent example of flexible polymeric material for intracortical probes [28–30]. Its key features are similar to those previously reported for parylene, including a low Young's modulus (1-3 GPa) and a simple integration in microfabrication

processes. Polyimide is available commercially in the form of ready-made films of different thicknesses (25-125  $\mu\text{m}$ , Kapton) or as a spin-coatable and curable solution (HD Microsystems), which can then be patterned through a standard dry etching step. It is known for its chemical resistance, can be used for electrical insulation applications and can maintain its properties over a wide range of temperatures [31]. Flexible polyimide probes have been tested *in vivo* to evaluate both the foreign body reaction and their recording ability. Cheung and coworkers [28] reported a PI-based microelectrode array with unaltered recording capability in rats up to 8 weeks and preliminary histology showing minimal tissue response. A comparative study carried out by Lee *et al.* [32] confirmed a reduced foreign body reaction in polymeric probes (including polyimide) compared to silicon probes, by analyzing five different targets of interest (microglia, activated microglia, blood-brain barrier leakiness, astrocytes and neuronal nuclei).

### Elastomeric substrates

Despite the improvements brought forth by the use of parylene and PI, academic research has been focusing in recent years on further reducing the mechanical mismatch with brain tissue. PDMS is an elastomer with a Young's modulus in the range of few MPa. Aside from being softer than the previously described substrates, it is also known for its compliance and stretchability, making it more suitable for dynamic neural tissue, such as the one found in the spinal cord. In 2015 Minev *et al.* [33] envisaged a completely soft and stretchable neural interface. The device, named e-dura, is composed of an elastomeric substrate, integrating stretchable micro-cracked gold interconnects and electrodes coated with a soft platinum-silicone composite (fig.2.2). E-dura was implanted below the dura mater in the spinal cord, showing desired conformability and low compression of tissue, compared to a stiff polyimide reference. Furthermore, the team confirmed a long-term (6 weeks) biocompatibility, through standard histological analysis and by highlighting unaltered motor functions of rats with soft implants, as opposed to those with PI interfaces, presenting visible motor deficits after just 1-2 weeks.

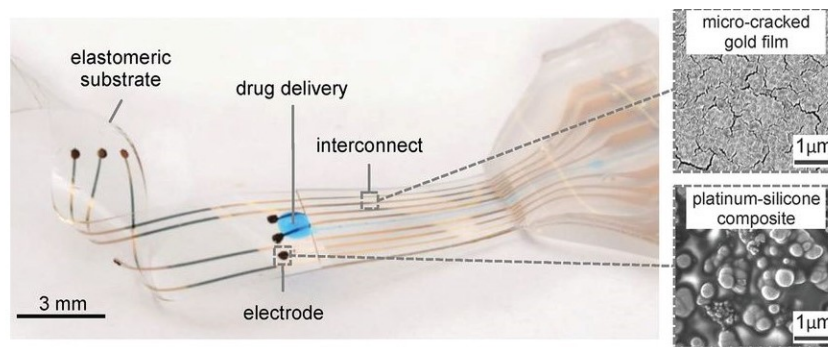


Figure 2.2 – **E-dura implant, with SEM inserts of interconnects and electrodes** [33]. Soft neural interface integrating a silicone substrate, stretchable interconnects, soft electrodes and a microfluidic channel for drug delivery.

When working with elastomeric interfaces special care must be taken when integrating metal electrodes, which are stiff and smooth by nature. A microcracked morphology is desirable in order to guarantee a certain degree of reversible stretchability and, at the same time, maintain electrical conductivity and a tight bonding to the underlying soft substrate [34].

The main limitation of PDMS as a neural interface material becomes apparent in its application to intracortical probes: as a very soft substrate it is not suitable for fabricating micro-scale penetrating probes, as it would easily undergo mechanical buckling during insertion.

## 2.2 Hydrogel/Polymer coatings

The implantation of a flexible probe can be aided through a number of strategies, which include the use of a stiff removable aid, coating with materials which soften in physiological conditions or with stiff bioresorbable polymers. Stiff shuttles however determine a larger insertion trauma; additional damage and possible dragging of the probe can also occur due to aid retraction [26], making other techniques preferable.

### Bioresorbable polymers

The concept of a bioresorbable coating is simple and effective: it consists in using free chains of polymers such as polyethylene glycol (PEG), poly(lactic-co-glycolic acid) (PLGA), collagen or silk (Young's modulus of a few GPa) as a temporary coating surrounding thin flexible probes [35]. The coating promotes insertion and degrades by dissolution when in physiological conditions, leaving the underlying substrate exposed to neural tissue.

There are however a number of limitations and concerns which must be taken into account when selecting a polymeric coating. For instance, coating degradation time, which generally varies between minutes and weeks, can be problematic both for initial insertion and during later time points after implantation. A fast-dissolving polymer may not be suitable for a slow accurate insertion process [26], while, on the other hand, a slow-dissolving polymer amounts to a thicker and relatively stiff probe being implanted for a number of days or weeks, inevitably causing more pronounced foreign body reaction. Another relevant issue is linked to the potential toxicity of degradation products, which needs to be accurately analyzed *in vitro* before implantation *in vivo* [36].

### Hydrogels

An alternative or complementary strategy to ensure probe softening consists in using low Young's modulus coatings. Hydrogels are a type of polymeric material which have been proposed for this specific application, as their mechanical and physical properties can be adjusted according to the chemical composition and cross-linking network. Hydrogels can be fabricated from natural materials (e.g. alginate, collagen, fibrin), which promote cellular interactions, or from synthetic materials (e.g. polyvinyl alcohol, polyethylene glycol), whose composition and properties are more easily controllable and which can incorporate bioactive elements to enhance cell attachment [37]. By properly tailoring the composition it is possible to obtain materials with a Young's modulus of hundreds of kPa to few MPa in the hydrated state. Hydrogels can thus act as a buffer layer between stiff electrodes and soft tissue. However, hydrated hydrogels also undergo significant swelling (fig 2.3), leading to an increase in distance between electrodes and target neurons, ultimately causing a loss in recording functionality, as shown by Kim and coworkers [38]. In terms of biocompatibility, Spencer *et al.* [18] reported a reduced scarring at different chronic time points by coating borosilicate probes with polyethylene glycol dimethacrylate (PEG-DMA) hydrogels. However, they also noted that thick coatings, which increase the overall size of the probes, lead to a tradeoff between the beneficial effect of a soft

material and the detrimental effect of an increased footprint.

The biocompatibility of hydrogels has already been extensively analyzed for different biomedical applications, including tissue engineering and the fabrication of contact lenses [39]. Years of research in the field of tissue engineering have also favored the optimization of a number of dispensing and patterning techniques, from 3D bioprinting to electrospinning [40]. Limited studies have instead been carried out to investigate the potential integration of hydrogels in intracortical probes. Hydrogels are commonly dispensed on stiff probes through a simple dip-coating approach. Both sides are coated with a thickness which depends on hydrogel composition, coating and retraction speed [26].

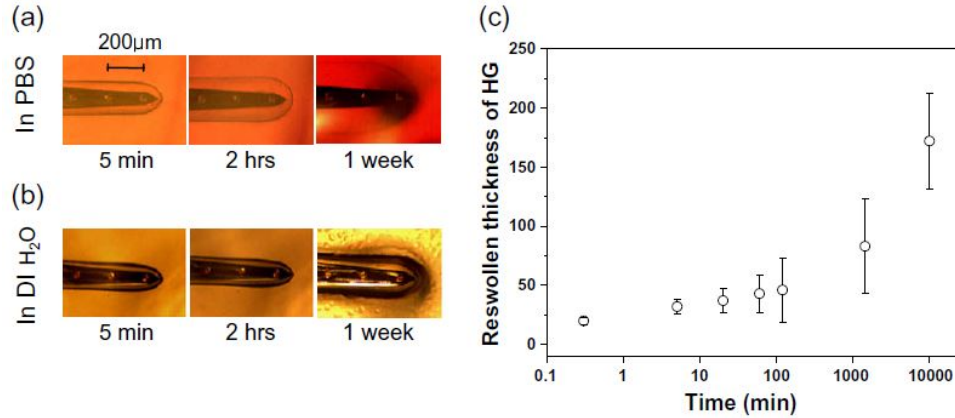


Figure 2.3 – **Reswelling of alginate coating on silicon probes in agar** [38]. Optical images of alginate reswelling over 1 week in phosphate buffered saline (PBS) (a) and deionized water (DI) (b). Reswelling of coating (original thickness 50 μm) in PBS agar (c).

On the other hand, micro-patterning of hydrogels on neural implants and other microsystems cannot rely on methods employed in tissue engineering, such as 3D bioprinting, as the resolution of such techniques is currently in the order of hundreds of microns. A possible solution consists in photocrosslinking monomers and photoinitiator using a photomask to define a pattern, yielding a resolution better than 10 μm [41]. Lei *et al.* [42] achieved a resolution of 2.5 μm through a photolithographic step, suitably adjusted to avoid any possible hydrogel swelling, followed by a standard dry etching.

These techniques have been developed for potential applications to microsensor and microactuator systems, yet they remain to be tested in an applied hydrogel-based device, such as an intracortical probe for neural sensing.

## 3 Materials and methods

### 3.1 PHEMA hydrogel preparation

In all steps of the project the following protocol was used for the preparation of hydrogel. All chemicals were provided by Sigma-Aldrich.

The synthesis of poly(2-hydroxyethyl methacrylate) (PHEMA) hydrogel (fig. 3.1) was carried out in pure ethanol by free radical polymerization of 60 wt.% of 2-hydroxyethyl methacrylate (HEMA) monomer with 0.2 mol % of ethylene glycol dimethacrylate (EGDMA) crosslinker. The thermal initiator azobisisobutyronitrile (AIBN) was finally added (0.1 mol %) and dissolved in the solution. The obtained pre-gel solution was conserved at  $-25^{\circ}\text{C}$ .

PHEMA was dispensed either through spin coating or casting on  $50\ \mu\text{m}$  PET sheets. To increase the viscosity of the solution an ultraviolet (UV) initiator, 2-hydroxy-2-methylpropiophenone ( $17.5\ \mu\text{L/g}$ ), was added. The solution was photoinitiated at  $365\ \text{nm}$  for 5 minutes, before dispensing. Polymerization was carried out either thermally ( $80^{\circ}\text{C}$  for at least 2 hours) or through UV treatment ( $365\ \text{nm}$  for 10 to 30 minutes).

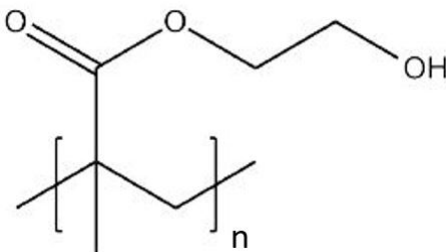


Figure 3.1 – **Molecular structure of poly(2-hydroxyethyl methacrylate)**. Hydrogel obtained from polymerization of 2-hydroxyethyl methacrylate monomer.

### 3.2 Material study and integration for passive probes

Experiments were conducted to characterize properties of polyimide and the PHEMA hydrogel both as plain materials and when integrated in a multilayered structure. Mechanical behavior was analyzed in terms of film folding and conformability, adhesion strength and buckling. These tests were performed in order to design and fabricate an intracortical probe with properly grafted substrate and coating, high conformability to soft neural tissue and, simultaneously, sufficient thickness and stiffness to guarantee a successful insertion in rat cortex. *In vivo* experiments were carried out to monitor tissue response to the proposed hydrogel-coated probe.

#### 3.2.1 Conformability study

Material conformability allows an optimal coupling of the penetrating neural interface to brain tissue and is associated with lower tissue compression and damage.

Capillary wrapping is the mechanism responsible for sheets of material conforming to underlying wet 3D structures such as cylinders or spheres, which represent the curved geometry of brain tissue. The folding of a plate of material of length  $L$  on a wet cylinder of radius  $R$  is determined by the competition between two energies: the surface energy of the wet structure,  $\gamma L$  (where  $\gamma$  is the surface tension), and the elastic bending energy of the plate  $\frac{BL}{2R^2}$ , where  $B = \frac{Eh^3}{12(1-\nu^2)}$  is the bending stiffness, which depends on geometrical

and mechanical parameters ( $h$ =membrane thickness,  $E$ =Young's modulus,  $\nu$ =Poisson's ratio) [43]. The balance between these energies is expressed through their ratio, which leads to a critical value of surface tension and to the definition of the critical thickness below which a material will fold:

$$\gamma_c = \frac{EI}{2R^2} \quad (1)$$

$$h_c = \sqrt[3]{\frac{24R^2(1-\nu^2)\gamma}{E}} \quad (2)$$

A similar reasoning can be applied to the case of a circular film of radius  $r$  wrapping around a sphere with radius  $R$  at a critical adhesion energy [44]:

$$\gamma_c = \frac{EI}{R^2} + \frac{Eh}{r^2} \int_0^r \left(1 - \frac{R}{x} \sin \frac{x}{R}\right)^2 x dx \quad (3)$$

It is then possible to define the critical thickness as that for which  $\gamma_c < \gamma = 10 \text{ mJ/m}^2$ , an adhesion energy per unit area value extracted experimentally [44].

Theoretical critical thicknesses were defined for three materials with different Young's moduli (fig. 3.2): PHEMA hydrogel in the wet state ( $E \approx 220 \text{ kPa}$ ), PDMS ( $E \approx 1 \text{ MPa}$ ) and PI ( $E \approx 2 \text{ GPa}$ ).

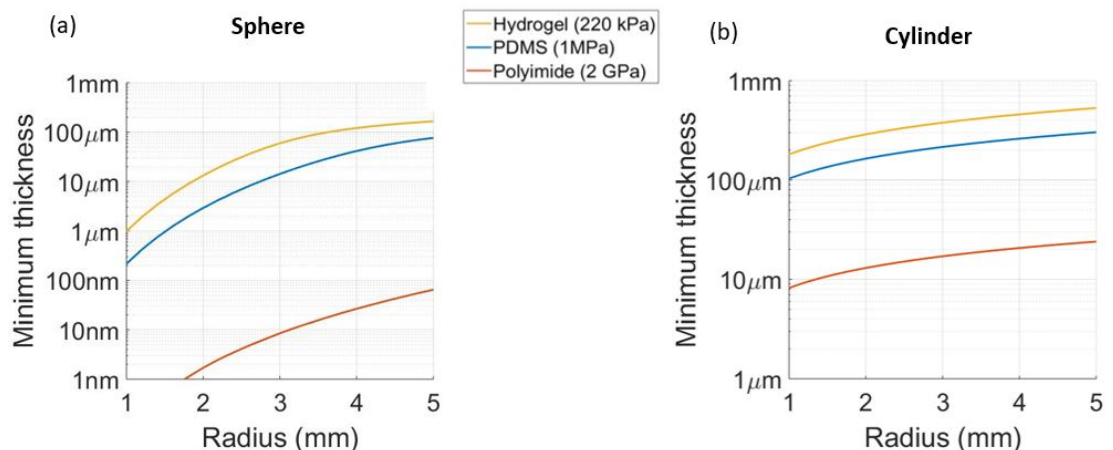


Figure 3.2 – **Conformability of different thicknesses of PHEMA, PDMS and PI.** Theoretical thickness below which a circular film conforms to a spherical structure (a) and a rectangular plate conforms to a cylindrical structure (b).

An experimental conformability study was conducted to validate the theoretical curves. Spherical and cylindrical structures with a wet surface were fabricated by preparing an agarose solution (3% w/v, Patisier Agar Agar) shaped in custom-made molds with varying radii ( $R = 2 \text{ mm}, 3 \text{ mm}, 4 \text{ mm}$ ). Circular and rectangular films of different dimensions were tested on the agarose structures and conformability or lack thereof was observed. Circular films with radii  $r = 1.75 \text{ mm}, 2 \text{ mm}, 2.5 \text{ mm}$  and rectangular films with  $L = 10 \text{ mm}$  were prepared.

PDMS samples were fabricated on silicon wafers. A release layer of poly(4-styrenesulfonic acid) solution (PSS, Sigma-Aldrich) was spin coated and baked. PDMS (10:1 base-curing agent ratio, Sylgard 184) was then spin coated at different speeds and baked to obtain desired thicknesses. Rectangular and circular shapes were laser cut (WS Turret, Optec Laser System) and released from the wafer.

PI samples were also prepared on wafer, with the exception of thick samples which were laser cut from prepared films (25  $\mu\text{m}$  Kapton). A thin sacrificial aluminum layer was sputtered, followed by spin coating and baking of a polyimide resin (PI 2611, HD Microsystems). PI shapes were defined through patterning of a photoresist mask and dry pure  $\text{O}_2$  plasma etching. Structures were finally released in a NaCl solution through an anodic dissolution process.

PHEMA samples were instead prepared either through casting on 50  $\mu\text{m}$  PET sheets or by infusing the prepolymerized hydrogel solution in pre-made PDMS gaskets (for thicknesses above 300  $\mu\text{m}$ ). After photocuring, desired shapes were laser cut.

The theoretical curve for polyimide on a spherical structure was not verified as the region of interest is in the nm scale.

The conformability study was then repeated for a multilayered system. In the case of a cylindrical underlying structure, equation 1 is still valid, but in this configuration the bending stiffness is defined by the mechanical and geometrical features of each layer [45]:

$$EI = \sum_{i=1}^n E_i h_i \left\{ \frac{h_i^2}{3} + \left[ \left( \sum_{j=1}^i h_j \right) - h_{neutral} \right]^2 - h_i \left[ \left( \sum_{j=1}^i h_j \right) - h_{neutral} \right] \right\} \quad (4)$$

where  $h_{neutral}$  represents the distance from the neutral plane.

The experimental study was performed on a multilayered system similar to the conceived probe structure, made of polyimide encapsulated in hydrogel (fig. 3.3). Polyimide samples of 10  $\mu\text{m}$  thickness were prepared and released as previously described.

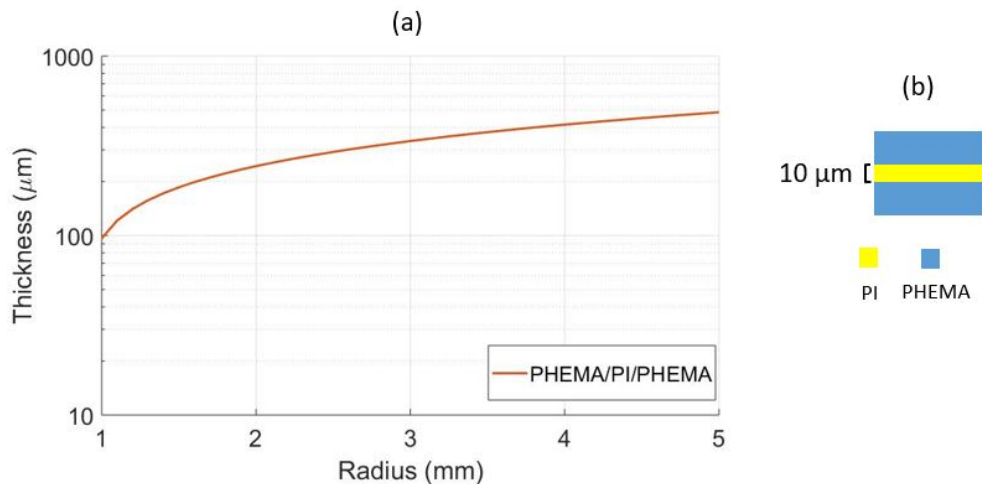


Figure 3.3 – **Conformability of a polyimide layer encapsulated in PHEMA.** Theoretical thickness below which a rectangular plate conforms to a cylindrical structure (a) in the case of a multilayered system PHEMA-PI-PHEMA (b).

They were then laminated on a layer of hydrogel cast on a PET sheet. After UV polymerization, the PI/PHEMA samples were laminated on a second layer of cast hydrogel. Final encapsulated films were laser cut and tested on cylindrical agarose structures.

### 3.2.2 Material integration: surface treatments

Suitable grafting of the hydrogel coating to the polyimide substrate is necessary to guarantee structural integrity and to avoid possible delamination during chronic implanta-

tion. Tests were performed on both plain and treated polyimide to identify the best method to obtain a reliable grafting. Pristine PI samples were compared to plasma-treated PI (Diener Electronic, 0.4 mbar, 30 W, 30 s) and samples subject to plasma treatment followed by a 3-(trimethoxysilyl)propyl methacrylate (TMSPMA, Sigma-Aldrich) hydrophilic silanization. Three different types of experiments were performed: contact angle measurements, T-peel tests and accelerated aging tests.

### **Contact angle measurements**

The wettability of pristine and treated PI layers (75  $\mu\text{m}$  Kapton film) was evaluated through contact angle measurements, which are commonly used to demonstrate the hydrophobic ( $90^\circ$ - $120^\circ$ ) or hydrophilic ( $<90^\circ$ ) nature of a given sample. Deionized (DI) water droplets (volume= $2\ \mu\text{L}$ ,  $n=4$  per sample) were dropped on the polyimide surface with the sessile drop technique.

Measurements for treated samples were performed immediately after treatment and were repeated at later timepoints (24 hours, 7 days) to observe the evolution of wettability over time.

### **T-peel tests**

T-peel tests were performed to evaluate the adhesive strength between two layers of polyimide bonded by a layer of PHEMA. Samples were fabricated by joining two films of 25  $\mu\text{m}$  thick PI with a layer of hydrogel ( $t_{dry} \approx 850\ \mu\text{m}$ ,  $w \approx 17\ \text{mm}$ ,  $l \approx 20.5\ \text{mm}$ ).  $N=4$  samples were tested for each different surface condition, both in the wet and the dry state. Polyimide extremities were peeled at a rate  $v = 0.5\ \text{mm/s}$  (MTS Criterion Model 42) and resulting Force vs Displacement curves were analyzed in terms of peak load and interfacial toughness, defined as the average force per unit width (fig. 3.4). Testing of completely swollen hydrogel was possible by using a wet chamber (Bionix EnviroBath) filled with DI water at room temperature.

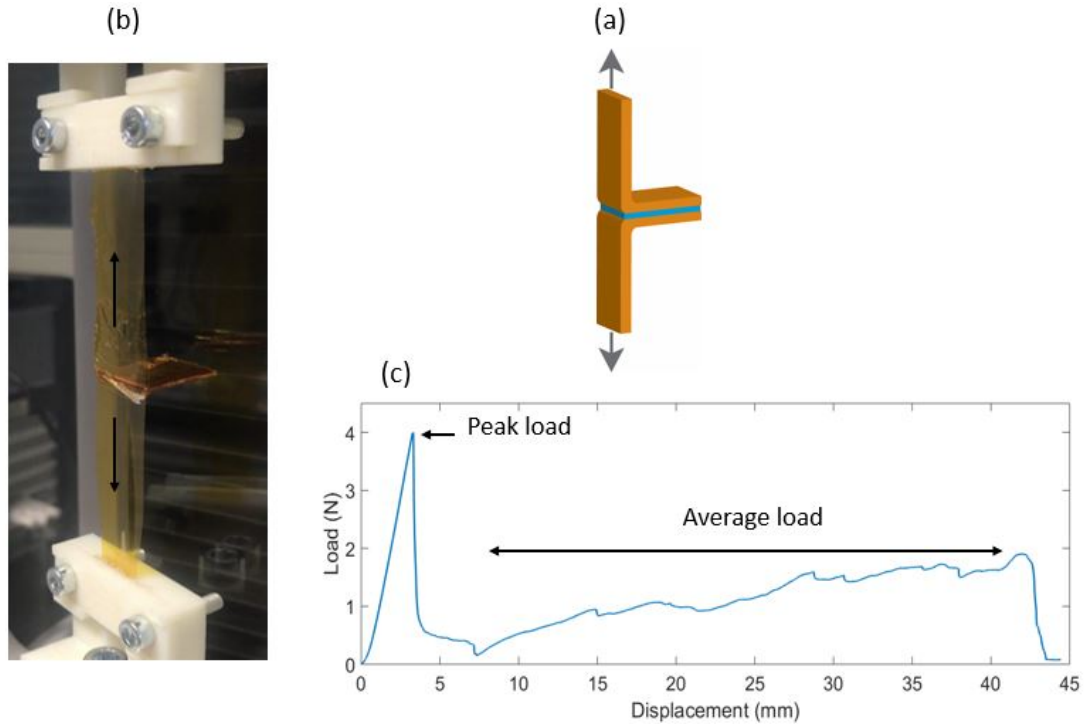


Figure 3.4 – **T-peel test for PI-PHEMA samples.** Schematic illustration (a) and actual setup (b) for T-peel testing of PI-PHEMA samples; analyzed output curve (c).

### Accelerated aging tests

Accelerated aging tests were performed on PI-PHEMA bilayers to monitor the sample degradation and possible delamination due to swelling. Hydrogel (caster setting at  $400\ \mu\text{m}$ ) was cast on a  $75\ \mu\text{m}$  thick polyimide film (pristine or treated). After UV curing samples were aged in  $0.1\ \text{M}$  PBS at  $55\ ^\circ\text{C}$  for 1 month. Morphological damage and possible delamination was observed through optical microscopy.

Plasma treated multilayers (PHEMA-PI-PHEMA) laser cut in probe shapes were left in agarose gel for a number of days. Initial weight was measured in the dry state on day 0 and then again at different timepoints in the dry state (day 1, 4, 6 and 7).

### 3.2.3 Probe design

A single-shank configuration (fig. 3.5) was used for the fabrication of hydrogel-coated polyimide probes, with geometrical features comparable to those found in literature ( $w = 300\ \mu\text{m}$ ,  $L = 3\ \text{mm}$ ) [21, 27, 46]. The proposed geometry is entirely based on a design previously developed within the research group. The overall thickness of the device was subsequently calculated based on mechanical considerations.

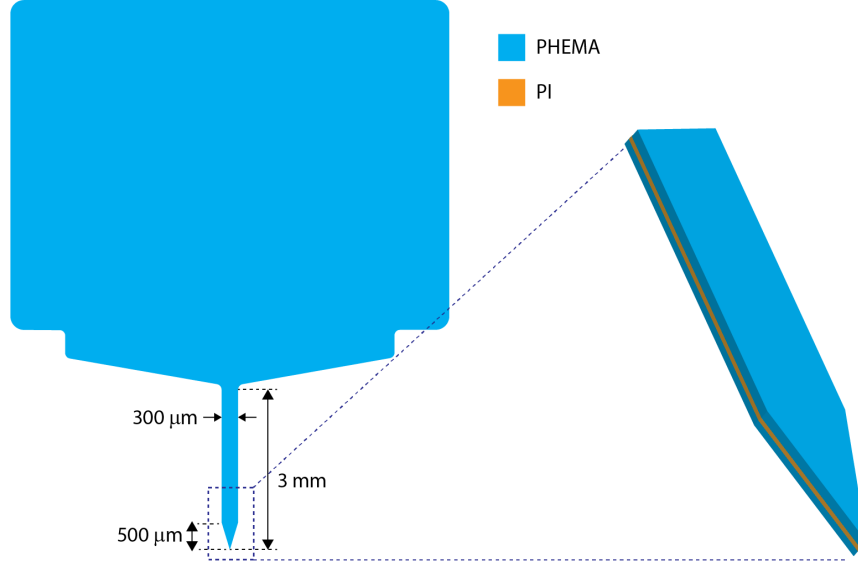


Figure 3.5 – **Schematic illustration of passive probe design.** Single-shank ( $w=300\ \mu\text{m}$ ,  $L=3\ \text{mm}$ ) design for multilayer PHEMA-PI-PHEMA probe.

### 3.2.4 Theoretical model and simulation

An accurate mechanical analysis is necessary to define probe dimensions, especially in the case of flexible materials, as they can easily undergo buckling. When probes enter the brain tissue, they are subject to a penetration force which can cause the system to fail.

Experimental studies carried out on rat brains have led to a general consensus regarding the entity of the penetration force for a variety of tip shapes and cross-sections. Jensen *et al.* [47] reported an insertion force in the range 0.48-1.15 mN for silicon and tungsten probes with different tip opening angles and cross section geometries (rectangular and circular). Similar results were obtained by Sharp and coworkers [48] (0.54-2.48 mN) for cylindrical stainless steel probes with diameters varying from 100  $\mu\text{m}$  to 200  $\mu\text{m}$ . One group based their design of parylene probes on the assumption of a penetration force range of 500-1000  $\mu\text{N}$  [49].

Theoretically, to have a successful insertion, the penetration force should be lower than the critical buckling load of the probe. This mechanical problem is commonly addressed by referring to the buckling model of a fixed-pinned beam. The critical buckling load, applied to the pinned end, is defined as:

$$F_{cr} = \frac{\pi^2 E b h^3}{5.88 L^2} \quad (5)$$

where  $E$  =Young's modulus,  $b$  =beam width,  $h$  =beam thickness (smallest dimension),  $L$  =beam length.

To better understand the mechanical failure in the case of a multilayered system, a 3D finite element model was developed using COMSOL Multiphysics 5.3. The model consisted of a single component: the probe shank ( $w = 300\ \mu\text{m}$ ,  $L = 3\ \text{mm}$ ) with a sharp tip geometry. The fixed-pinned buckling condition was approximated by fixing the top end of the probe, while applying a  $F = 1\ \mu\text{N}$  load to the tip, which was also allowed to rotate. By performing a linear buckling analysis, the critical load factor  $k_{cr}$  was derived

and multiplied to the original load, to obtain the critical buckling load  $F_{cr} = k_{cr}F$ . The accuracy of the physics applied to the model was confirmed by comparing theoretical values to simulated mono-material beams.

The described simulation was performed on different probe configurations: a PHEMA-PDMS-PHEMA multilayer (fig. 3.6a), a single PI layer (fig. 3.6b), and a PHEMA-PI-PHEMA multilayer (fig. 3.6c). The first two were simulated at a constant thickness (25  $\mu\text{m}$  PI, 120  $\mu\text{m}$  multilayer) and varying width ( $w = 100 \mu\text{m}, 200 \mu\text{m}, 300 \mu\text{m}$ ), while the latter was kept at a constant width ( $w = 300 \mu\text{m}$ ) and varied in hydrogel coating thickness (2-20  $\mu\text{m}$  on each side). Mechanical properties were defined for each material (table 1). PHEMA was simulated in the dry condition, corresponding to its state prior to insertion, in which it has a Young's modulus of approximately 8 GPa. In the wet condition, corresponding to the post-insertion state, it instead has a low modulus in the range of 220 kPa.

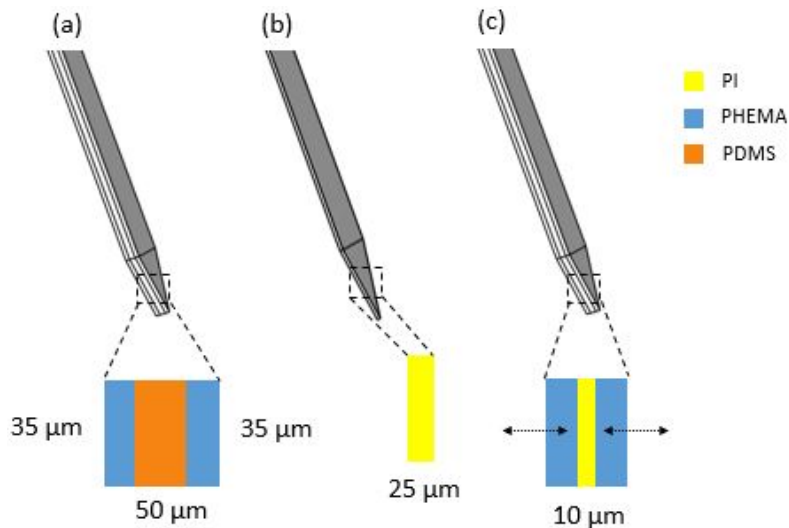


Figure 3.6 – **Schematic illustration of simulated probes.** PHEMA-PDMS-PHEMA (a) and PI (b) probes with constant thickness and varying width ( $w=100 \mu\text{m}, 200 \mu\text{m}, 300 \mu\text{m}$ ), PHEMA-PI-PHEMA probe with constant width ( $w=300 \mu\text{m}$ ) and varying coating thickness (2-20  $\mu\text{m}$  per side).

Table 1 – **Material properties used in finite element model.**

Material	Young's modulus	Poisson's ratio	Density
PDMS	1.5 MPa	0.49 [50]	970 kg/m <sup>3</sup>
PI	1.5 GPa	0.33 [51]	1300 kg/m <sup>3</sup>
PHEMA (dry)	8 GPa	0.29 [52]	1050 kg/m <sup>3</sup>

The PHEMA-PDMS-PHEMA and PI configurations were used for a first buckling simulation, performed to validate the model. Results were compared to experimental insertion tests, carried out both *in vivo* and in an agarose phantom brain, fabricated as detailed above.

A second analysis was performed exclusively on the PHEMA-PI-PHEMA model to determine suitable hydrogel coating thickness to ensure a successful probe insertion. An insertion force range of 500-1000  $\mu\text{N}$  was selected for this study, in accordance with Wester *et al.* [49].

### 3.2.5 Fabrication method

Single-shank passive probes consisting of alternating layers of PHEMA-PI-PHEMA were fabricated for *in vivo* experiments.

Titanium (25 nm, adhesion layer) and a sacrificial aluminum layer (100 nm) were sputtered (AC450, Alliance Concept) on a 4 inch carrier silicon wafer. A 5  $\mu\text{m}$  layer of polyimide resin (PI 2611, HD Microsystems) was spin coated (2500 rpm, 60 s), baked (70  $^{\circ}\text{C}$ , 3 min, then 110  $^{\circ}\text{C}$ , 3 min) and finally cured in nitrogen atmosphere (300  $^{\circ}\text{C}$  for 1 hour). A second layer of polyimide was coated and cured as before over the first one, to obtain a total thickness of 10  $\mu\text{m}$ . A 12  $\mu\text{m}$  layer of photoresist (AZ 9260, MicroChemicals) was spin-coated (1500 rpm, 40 s), soft-baked (110  $^{\circ}\text{C}$ , 6 min), exposed (MLA150, Heidelberg Instruments, 440  $\text{mJ}/\text{cm}^2$ , 405 nm) and developed (AZ 400K, 9 min). The resist was used as a mask for a RIE  $\text{O}_2$  dry etching step (Corial 210IL, Corial,  $\text{O}_2$  50 sccm, He 15 sccm, RF forward power 150 W, LF forward power 500 W). Polyimide was thus patterned in isolated shapes and a high area of underlying Al was exposed. Polyimide was released from the wafer (fig. 3.7-1) through an anodic dissolution process in a 18 g/L NaCl solution (2 V applied between Al and Pt counter electrode).

Released samples were washed in DI water, then laminated on a 50  $\mu\text{m}$  PET sheet and were allowed to dry while flat. The top face of PI then underwent a surface treatment, either an  $\text{O}_2$  plasma (0.4 mbar, 30 W, 30 s) or successive plasma treatment and TMSPMA silanization. Simultaneously a layer of photoinitiated pre-gel PHEMA was cast (caster setting 150  $\mu\text{m}$ ) on a 50  $\mu\text{m}$  PET sheet (fig. 3.7-2). The treated side of PI was then carefully laminated on the hydrogel, which was successively photocured. The exposed PI surface was treated either through plasma or plasma-silanization to promote the PHEMA-PI grafting. A second layer of photoinitiated pre-gel was then cast on the PET-PHEMA-PI stack (caster setting 180  $\mu\text{m}$ ) and photocured. As a final step the PET-PHEMA-PI-PHEMA stack was laser cut (WS Turret, Optec Laser System) to define probe shapes. Tweezers were used to peel hydrogel-encapsulated PI probes from the PET sheet. Samples were placed between PET sheets and metal plates to maintain them flat and were kept at 80  $^{\circ}\text{C}$  to ensure complete hydrogel drying. Total device thickness and all intermediate thicknesses were verified through mechanical profilometry (DEKTAK-XT, Bruker).

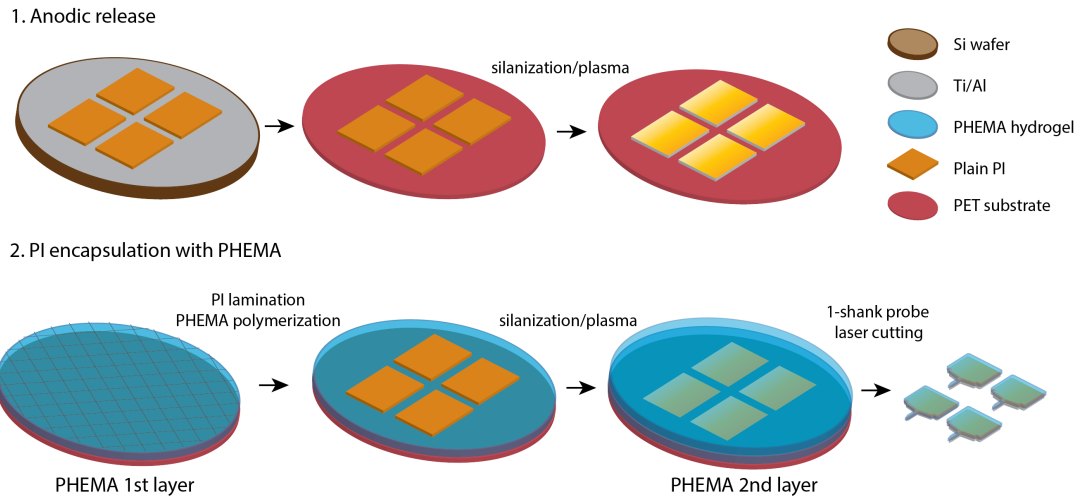


Figure 3.7 – **Process flow for PI release and hydrogel encapsulation.** After standard PI microfabrication, patterned samples were released (1) and laminated on PET. Encapsulation (2) between two hydrogel layers was obtained by successively treating PI surface and casting PHEMA on each side; final probe shapes were laser cut.

### 3.2.6 *In vivo* surgery

All surgical procedures and animal experiments were conducted in accordance with Swiss federal legislation and following protocols established at EPFL and approved by Swiss Veterinary Offices. A total of 2 rats (female Lewis rats) were used for the implantation of passive devices. Two types of probes (PHEMA-PI-PHEMA and PHEMA-PDMS-PHEMA multilayers), one per hemisphere, were implanted in each animal. PI-based devices had a total thickness of approximately 50  $\mu\text{m}$ , while PDMS-based implants had a total thickness of 125  $\mu\text{m}$ . Prior to surgery, all implants were sterilized with UV-ozone treatment (Uvfab Systems) for 30 s on each side, then kept in a dessicator to avoid hydrogel swelling. The animal was anesthetized with isoflurane gas and its head was shaved. The animal was then fixed to a stereotactic station. Two craniotomies were performed, one per hemisphere (fig. 3.8a). Dura mater was removed and a polyimide mask was positioned to guide implantation in the motor cortex. Probes were kept in a custom-made holder and lowered to penetrate the brain surface (fig. 3.8b). After implantation, probes were fixed to the skull using Kwik-Sil (World Precision Instruments) and dental cement (ProBase Cold, Ivoclar Vivadent) (fig. 3.8c). The skin around the scalp was sutured. The rat was then placed on a heated pad during recovery.

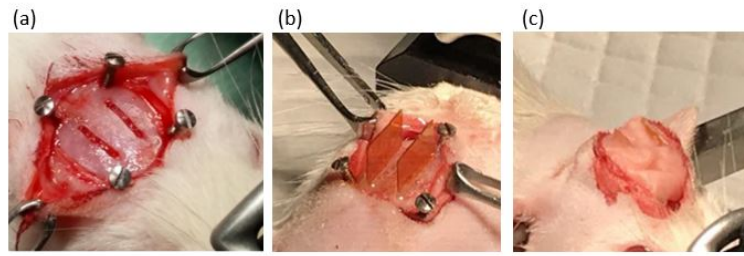


Figure 3.8 – **Surgical procedure for probe implantation.** One craniotomy performed for each hemisphere (a). One PHEMA-PDMS-PHEMA and one PHEMA-PI-PHEMA probe inserted through craniotomy mask (b). Probes fixed using Kwik-sil and dental cement; skin sutured (c).

### 3.2.7 Tissue processing and immunohistochemistry

After 7 days of implantation, the animals were anesthetized and perfused. After perfusion the devices were removed from the brain. Tissue was fixed in 4% paraformaldehyde (PFA) for 24 hours, then cryoprotected in a 30% sucrose solution in 0.1 M PBS until sinking occurred (72 hours). Brains were frozen at  $-60^{\circ}\text{C}$ , embedded in optimal cutting temperature (OCT) compound (Tissue-Tek) and preserved at  $-20^{\circ}\text{C}$  until slicing. Coronal sections ( $40\ \mu\text{m}$  thickness) were collected using a cryostat (Leica Microsystems) at  $-22^{\circ}\text{C}$ . Slices were mounted on slides and conserved at  $-20^{\circ}\text{C}$  prior to immunohistochemical labeling.

Immunostaining was carried out on the obtained slices. Half of them were labeled for neuronal nuclei and for astrocytes. Slices were rinsed in 0.1 M PBS, to remove OCT. Blocking was performed for one hour at room temperature in goat serum blocking solution (5% serum, 1% Triton-X 100 (Sigma-Aldrich) in 0.1 M PBS), to reduce nonspecific staining. The sections were then incubated overnight at  $4^{\circ}\text{C}$  in primary antibody solution. Mouse anti-neuronal nuclei (NeuN) (1:300, Millipore) were used as a marker for neurons, while rabbit antiglial fibrillary acidic protein (GFAP) (1:1000, Dako) was used to identify astrocytes. The tissue was rinsed again in 0.1 M PBS and stained with secondary antibodies in goat serum blocking solution (1% Triton-X 100, 2% serum in 0.1 M PB). Antibodies used were: goat anti-mouse 555 (1:300, Life Technologies) and goat anti-rabbit alexa 488 (1:400, Life Technologies).

The other half of the total slices were stained for microglia. Blocking of the tissue was performed for one hour at room temperature in donkey serum blocking solution (10% serum, 1% Triton-X 100 in 0.1 M PBS). Slices were incubated overnight at room temperature in primary antibody solution. The primary antibody used was rabbit anti-Iba1 (1:1000, Wako) for microglia. The tissue was rinsed again in 0.1 M PBS and stained with donkey anti-rabbit IgG (1:200, Life Technologies) in 0.1 M PBS + 0.3% Triton-X 100). Finally, all slides were washed with PBS, dried and coverslips were mounted with Mowiol antifade medium.

Immunolabeled fluorescent images were acquired using confocal microscopy (Zeiss LSM 880). Staining for a PHEMA-PI-PHEMA probe was qualitatively compared to PHEMA-PDMS-PHEMA and a silicon probe from a previous short-term (7 days) *in vivo* test.

### 3.3 Design and fabrication of electroactive probes

In the following the transition from a passive non-recording device used for a biointegration study, to an electroactive probe for long-term stable neural sensing is reported. The work presented is not only limited to the design of the probe itself, but mainly focuses on the development of a method to integrate PHEMA in a standard microfabrication process. This implies the optimization of an entirely dry process for the hydrogel patterning, as any contact with water causes a 27% swelling in volume, while hydration and successive dehydration lead to the formation of cracks and other surface irregularities, mainly when the hydrogel is constrained to a stiff substrate. The proposed method was used to fabricate probes and preliminary *in vitro* and *in vivo* tests were carried out to verify device functionality.

#### 3.3.1 Probe design

The soft hydrogel-coated intracortical probe (fig. 3.9) consists in a single-shank device incorporating single or multiple (2 or 3) Pt recording sites with a 100  $\mu\text{m}$  diameter. Platinum tracks (30  $\mu\text{m}$  wide), pads and recording contacts are encapsulated between two layers of polyimide, 5  $\mu\text{m}$  thick each. The entire system is surrounded by a mechanically-adaptive PHEMA coating. Contacts are opened through the top polyimide and hydrogel layers, to expose the underlying platinum electrodes. As a final step to enhance recording, a conducting hydrogel-based ink is printed on the platinum. The composite, based on polyacrylamide (PAAm) and poly(3,4-ethylenedioxythiophene) polystyrene sulfonate (PEDOT:PSS), completes the entirely soft penetrating neural probe. Formulation and dispensing of the composite was carried out entirely by a second member of the research group.

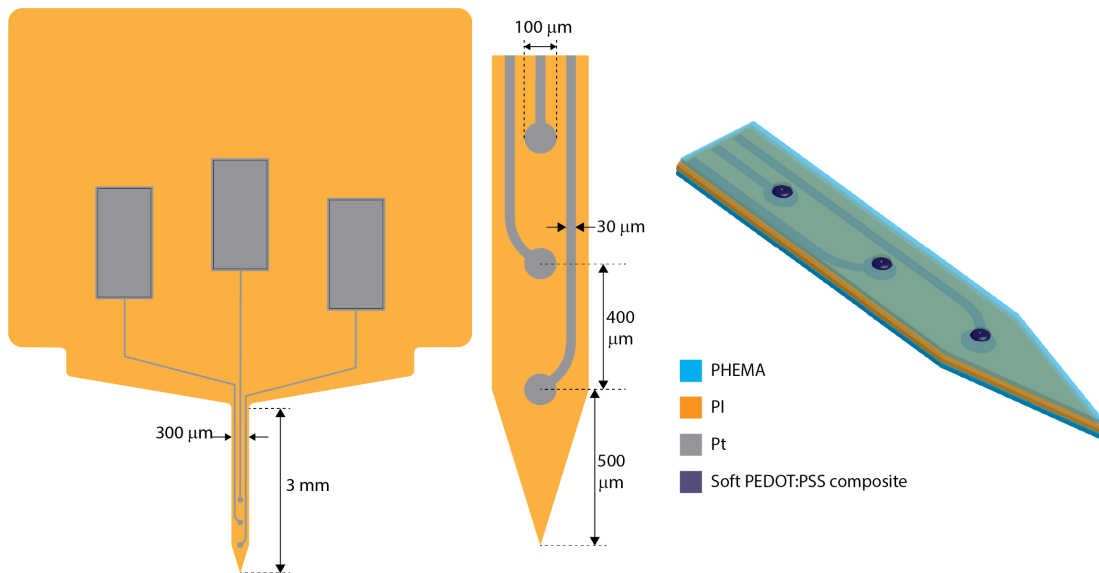


Figure 3.9 – **Schematic illustration of electroactive probe.** Design of an entirely soft active probe with 100  $\mu\text{m}$  Pt electrodes encapsulated in polyimide and hydrogel, and coated with a conductive hydrogel-based ink.

### 3.3.2 Fabrication method

#### Polyimide-platinum-polyimide microfabrication process

Electroactive probes were fabricated on a 4 inch carrier silicon wafer. As a first step, the encapsulation of platinum tracks in polyimide was carried out through a standard microfabrication process. Titanium (25 nm, adhesion layer) and a sacrificial aluminum layer (100 nm) were sputtered (fig. 3.10a). A 5  $\mu\text{m}$  layer of polyimide resin (PI 2611, HD Microsystems) was spin coated (2500 rpm, 60 s), baked ( $70^\circ\text{C}$ , 3 min, then  $110^\circ\text{C}$ , 3 min) and finally cured in nitrogen atmosphere ( $300^\circ\text{C}$  for 1 hour) (fig. 3.10b). Metal electrodes were fabricated by sputtering Ti (16 nm, adhesion layer) and Pt (150 nm). A 2.5  $\mu\text{m}$  photoresist mask (AZ 1512, MicroChemicals) was spin coated (1175 rpm, 40 s), baked ( $110^\circ\text{C}$ ), exposed ( $124\text{ mJ}/\text{cm}^2$ , 405 nm) and developed (AZ 726MIF, MicroChemicals, 60 s). Ti and Pt were etched using a  $\text{Cl}_2$ -based dry etching ( $\text{Cl}_2$  20 sccm, Ar 30 sccm, He 15 sccm, RF forward power 50 W, LF forward power 800 W) (fig. 3.10c). A second layer of polyimide was coated and cured as before over the first one, to encapsulate the platinum (fig. 3.10d). A 12  $\mu\text{m}$  layer of photoresist was coated and patterned to mask the underlying layer during the dry  $\text{O}_2$  etching of 10  $\mu\text{m}$  polyimide, following the same process presented in section 3.2.5 (fig. 3.10e). As a result, a sufficiently large area of Al was exposed to ensure an efficient anodic release. Contacts and pads were opened through the polyimide layer with an additional photolithographic step. A 6  $\mu\text{m}$  layer of photoresist (AZ 9260, MicroChemicals) was spin coated (5000 rpm, 40 s), baked ( $110^\circ\text{C}$ , 3 min), exposed ( $300\text{ mJ}/\text{cm}^2$ , 405 nm) and developed (AZ 400K, MicroChemicals, 4 min). Finally,  $\text{O}_2$  etching was employed to expose the Pt (fig. 3.10f). In all photolithographic steps, photoresist was stripped in acetone.

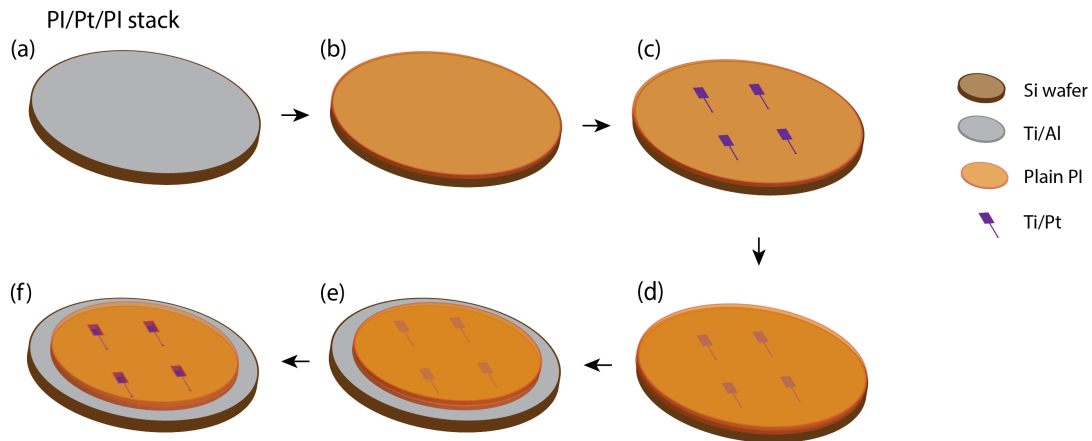


Figure 3.10 – **Process flow for PI/Pt/PI stack.** Ti/Al sacrificial layer sputtering (a), PI coating (first layer) (b), Pt sputtering and patterning (c), PI coating (second layer) (d), PI etching for Al exposure (e), PI etching for pad/contact opening (f).

#### PHEMA dispensing and etching

The critical step in the fabrication of hydrogel-based active probes is the patterning of the hydrogel itself, due to its incompatibility with standard wet processes, previously detailed. Consequently, two different methods were tested to etch hydrogel without compromising its dehydrated state. After an  $\text{O}_2$  plasma treatment (0.4 mbar, 30 W, 30 s), a

20-25  $\mu\text{m}$  layer of hydrogel was spin coated on the wafer (400 rpm, 60 s) and thermally cured (80  $^{\circ}\text{C}$  for 2 hours) (fig. 3.12a). Aluminum was protected with kapton tape during spin coating, to provide a reference for a successive measurement of the hydrogel thickness. As the viscosity of PHEMA pregel is significantly sensitive to environmental conditions (light and temperature), a certain variability in thickness (15-18%) is to be expected and requires close monitoring.

Preliminary testing of the etching methods was performed on plain silicon wafers with a spin coated layer of hydrogel. Masks for all methods were prepared with 100  $\mu\text{m}$ , 200  $\mu\text{m}$ , 300  $\mu\text{m}$  features to verify resolution (fig. 3.11a).

- The first method consisted in using polyimide-based shadow masks (fig. 3.11b) to be laminated directly onto the PHEMA. Four main configurations were prepared: 25  $\mu\text{m}$  PI, 75  $\mu\text{m}$  PI, 25  $\mu\text{m}$  PI with 100 nm Al coating, 25  $\mu\text{m}$  PI with 100 nm Al coating and a bottom thin PDMS adhesion layer.
- The second method was based on a technique proposed by Lei *et al.* [42], which consists in accurately underdeveloping photoresist to avoid any contact between the liquid developer and the underlying hydrogel (fig. 3.11c).

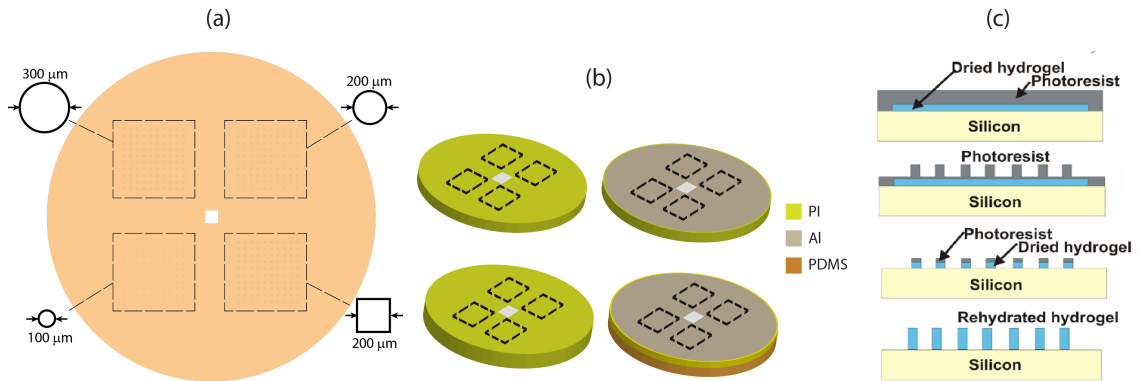


Figure 3.11 – **Methods for hydrogel etching.** Mask design to verify resolution of etching method (a), polyimide shadow mask configurations: plain PI, with or without protective Al layer and adhesive PDMS layer (b), underdeveloped photoresist method [42] (c).

As a result of poor contact to the hydrogel, mask delamination and mask etching, the polyimide shadow masks were not used to fabricate devices.

Hydrogel patterning (fig. 3.12b) was thus performed with the second method. A 14  $\mu\text{m}$  layer of photoresist (AZ 9260) was spin coated (1150 rpm, 40 s) and baked (110  $^{\circ}\text{C}$ , 7 min). Resist exposure was lowered from 490  $\text{mJ}/\text{cm}^2$ , the dose necessary to expose all 14  $\mu\text{m}$ . Exposure was carried out with 2 different methods: (1) all openings (recording sites and pads) were exposed with the same dose (340  $\text{mJ}/\text{cm}^2$ , 405 nm), (2) separate exposures were performed on large pads (340  $\text{mJ}/\text{cm}^2$ , 405 nm) and small contacts (290  $\text{mJ}/\text{cm}^2$ , 405 nm). Resist was then underdeveloped (AZ 400K, 6 min).  $\text{O}_2$  dry etching of PHEMA was carried out at a rate of approximately 2.7  $\mu\text{m}/\text{min}$  ( $\text{O}_2$  50 sccm, He 15 sccm, RF forward power 150 W, LF forward power 500 W). After exposing Pt, photoresist was stripped with a further  $\text{O}_2$  dry etching at lower power ( $\text{O}_2$  50 sccm, He 15 sccm, RF forward power 10 W, LF forward power 200 W), to limit Pt damage.

### Anodic release and encapsulation

The PI-PHEMA bilayer was released through anodic dissolution (fig. 3.12c) in an 18 g/L NaCl solution (2 V applied between Al and Pt counter electrode), the only wet step of the process. Released samples were washed in DI water, the backside was dried then treated with UV-ozone, as an alternative to O<sub>2</sub> plasma. PI-PHEMA was then laminated on a layer of hydrogel (250  $\mu$ m caster setting) which was cast on a PET sheet (fig. 3.12d-e). Hydrogel polymerization occurred through 30 minutes of UV treatment (365 nm). The soft composite material was dispensed through 3D bioprinting. Finally implants were laser cut (fig. 3.12f), peeled off from the PET sheet and kept between metal plates at 80 °C to maintain them flat and completely dry the hydrogel.

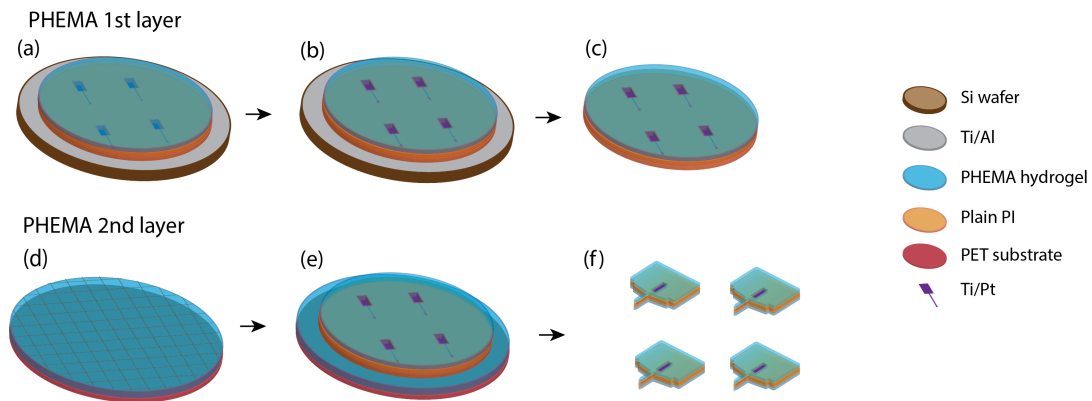


Figure 3.12 – **Process flow for encapsulation in hydrogel of PI/Pt/PI stack.** PHEMA spin coating and polymerization (a), PHEMA etching (b), anodic release of PI-PHEMA (c), PHEMA casting on PET sheet (d), lamination of PI-PHEMA stack on a second layer of PHEMA and polymerization (e), implant shaping through laser cutting (f).

### An entirely dry fabrication process

As an alternative to the previously described process for the fabrication of active probes, an entirely dry method was proposed, exploiting the poor adhesion which exists between polyimide and silicon. Polyimide was coated directly onto a bare silicon wafer and the PI/Pt/PI stack was generated and etched following the same steps (fig. 3.13a-f). In this configuration the complete 10  $\mu$ m layer of polyimide was etched either around the edges (fig. 3.13e) or already in defined probe shapes. This was done to directly remove critical areas of PI at the borders of the wafer, which could easily undergo a spontaneous delamination from silicon. Again, PHEMA was coated and patterned (fig. 3.13g-h). Probes were then laser cut and simply peeled off from the wafer using tweezers (fig. 3.13i). Released PI/Pt/PI/PHEMA stacks were then laminated onto a second layer of hydrogel and laser cut once more to obtain the final encapsulated probes (fig. 3.13j-l).

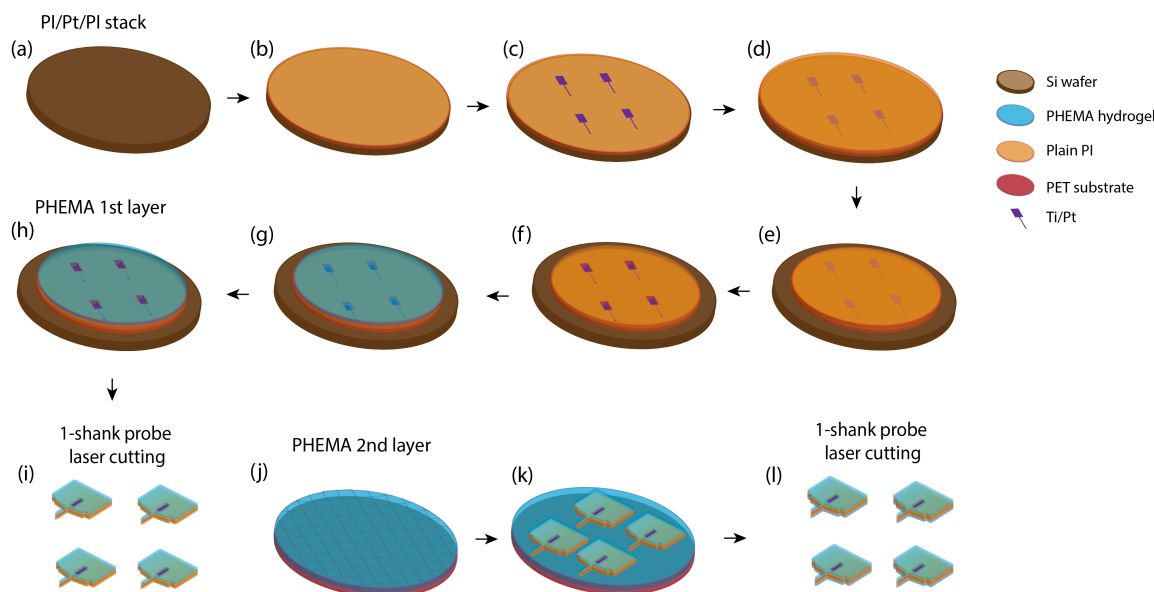


Figure 3.13 – **Dry process flow for the fabrication of active probes.** Bare silicon wafer (a), PI coating (first layer) (b), Pt sputtering and patterning (c), PI coating (second layer) (d), PI etching for probe shaping or edge removal (e), PI etching for pad/contact opening (f), PHEMA spin coating and polymerization (g), PHEMA etching (h), laser cutting and peeling of PI-PHEMA (i), PHEMA casting on PET sheet (j), lamination of PI-PHEMA stack on a second layer of PHEMA and polymerization (k), implant shaping through laser cutting (l).

The outcome of the fabrication process was monitored through optical microscopy, scanning electron microscopy (SEM, SU500 Hitachi) and energy-dispersive X-ray spectroscopy (EDS), mainly to evaluate the appropriate opening of Pt pads and contacts and their integrity.

### 3.3.3 Preliminary *in vitro* and *in vivo* tests

Fabricated implants were tested *in vitro* and *in vivo* to verify device functionality. Silver paste was dispensed on pads and connections were established using wires (CW6300, Cooner Wires). Alternatively, connectors (241050-4 - Pin header Male 8, Distrilec) were bonded to the electrode pads. RTV silicone was used to provide isolation. Wiring was performed by a second member of the research group.

### Electrochemical characterization

Cyclic voltammetry (CV) and impedance spectroscopy were carried out to evaluate electrode performance. Measurements were performed using a potentiostat (Gamry reference 600) in a 3-electrode setup (Pt working electrode, Ag/AgCl reference electrode, Pt counter electrode) immersed in a PBS solution. Impedance was evaluated in 61 frequency points from 1 Hz to 1 MHz by applying a 100 mV sinewave. CV measurements were performed applying voltage between  $-0.6$  V and  $0.8$  V at a scan rate of  $100$  mV/s, with a step size of  $2$  mV, repeated for 3 cycles. Data was analyzed for uncoated electrodes ( $n=6$ ).

### ***In vivo* acute surgery**

A preliminary recording test was performed on one Thy1-chr2-expressing female rat. The animal was prepared as described in section 3.2.6 and an active probe was implanted in the motor cortex. Two different stimulation methods were employed: (1) electrical stimulation of the sciatic nerve, (2) optical stimulation over the cortex, using a laser. Electrodes were connected to a recording system (Tucker Davis Technologies), which provided spike sorting and visualization, to verify neural activity in the cortex.

## 4 Results

### 4.1 Passive probes

#### 4.1.1 Conformability study

Theoretical conformability of three different materials (PI, PHEMA, PDMS) was confirmed experimentally on both cylindrical and spherical agarose structures (fig. 4.1). Overall, theoretical equations were verified in more than 90% of the cases, with limited exceptions for samples whose measured thickness varied by  $\pm 5 \mu\text{m}$  from the critical value.

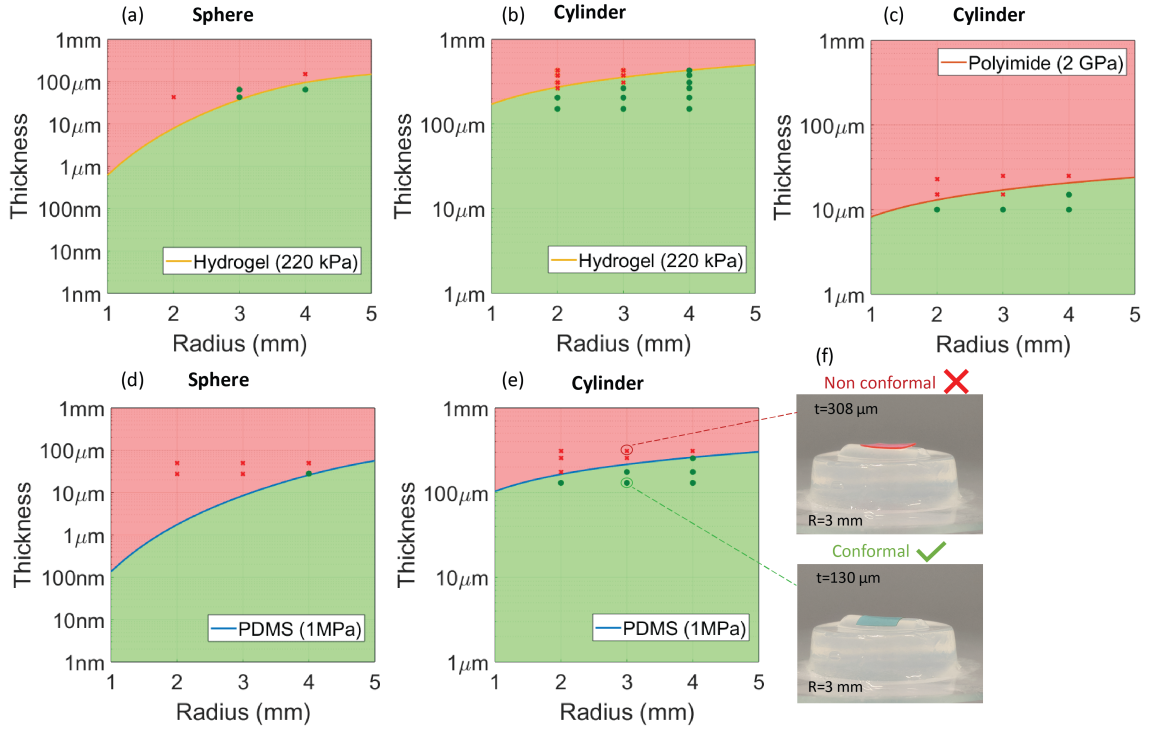


Figure 4.1 – **Experimental conformability of PHEMA, PI and PDMS.** Experimental conformability results for PHEMA (a-b), PI (c), PDMS (d-e) and examples of conformal and non-conformal PDMS samples (f).

The number and distribution of thicknesses evaluated per material in the conformal and non-conformal regions was dictated by practical manufacturing and handling limitations. PHEMA fabrication variability also yielded a higher number of samples which could be tested. A pronounced compliance of thick hydrogel sheets (hundreds of microns) was observed, highlighting a significantly different behavior compared to stiffer substrates. The influence of a  $10 \mu\text{m}$  layer of PI in a stack of PHEMA was analyzed in the second conformability study. Experimental tests, performed exclusively on cylindrical structures, once again confirmed theoretical predictions (fig. 4.2b-c) and further illustrated the beneficial effect of hydrogel. Despite the presence of a layer of stiff PI, the tested multilayer showed an improved performance compared to a typically conformal material, such as PDMS (fig. 4.2a).

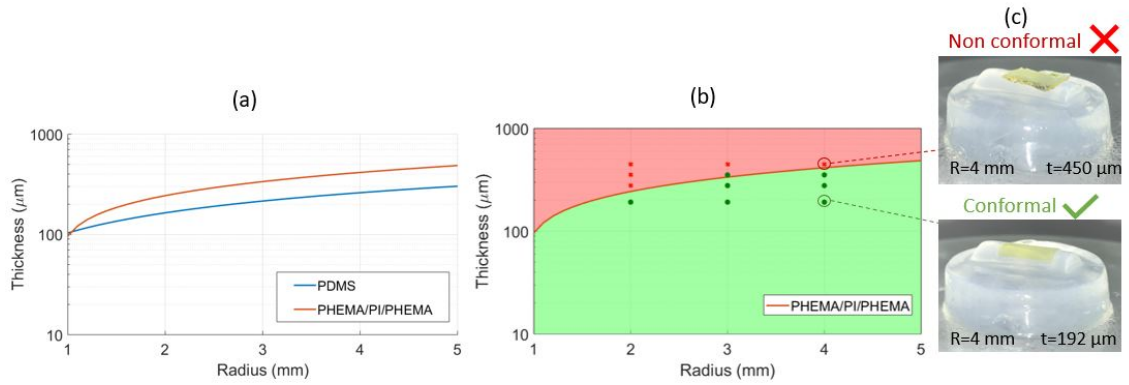


Figure 4.2 – **Theoretical and experimental conformability of PHEMA-PI-PHEMA.** Theoretical conformability of PHEMA-PI-PHEMA compared to plain PDMS (a), experimental results (b) and examples of conformal and non-conformal samples (c).

#### 4.1.2 Surface treatments

The adequate treatment of PI to favor the integration of hydrogel was analyzed through contact angle measurements, T-peel tests and aging tests.

The average water contact angle for plain PI was found to be  $78^\circ$ , indicating that the material is slightly hydrophilic in the pristine state. Surface treatments significantly lowered the contact angle value:  $29^\circ$  for plasma-treated samples, and  $31^\circ$  in the case of plasma followed by hydrophilic silanization (fig. 4.3a). The wettability of treated PI surfaces degraded over time and in a similar manner in both cases (fig. 4.3b). After 24 hours average contact angles were  $55^\circ$  (plasma) and  $56^\circ$  (plasma+TMSPMA), after 7 days they reached  $72^\circ$  (plasma) and  $68^\circ$  (plasma+TMSPMA).

The T-peel tests were performed to evaluate the adhesion and robustness of PI-PHEMA interfaces. The initial peak load (N) required to break the interface and the interfacial toughness, representing the average peel force per unit of width ( $\text{J}/\text{m}^2$ ), were analyzed and compared to two references: plasma-bonded PDMS and a system reported in literature consisting of PDMS bonded to a PAAm hydrogel layer undergoing a  $90^\circ$  peel test [53]. As expected, samples in the wet state showed a lower adhesion compared to their dry counterparts, regardless of the surface treatment: average peak loads lowered from 4.3 N to 3.2 N for pristine samples, from 7.7 N to 3.1 N for plasma and from 6.6 N to 3.5 N for TMSPMA (fig. 4.4a).

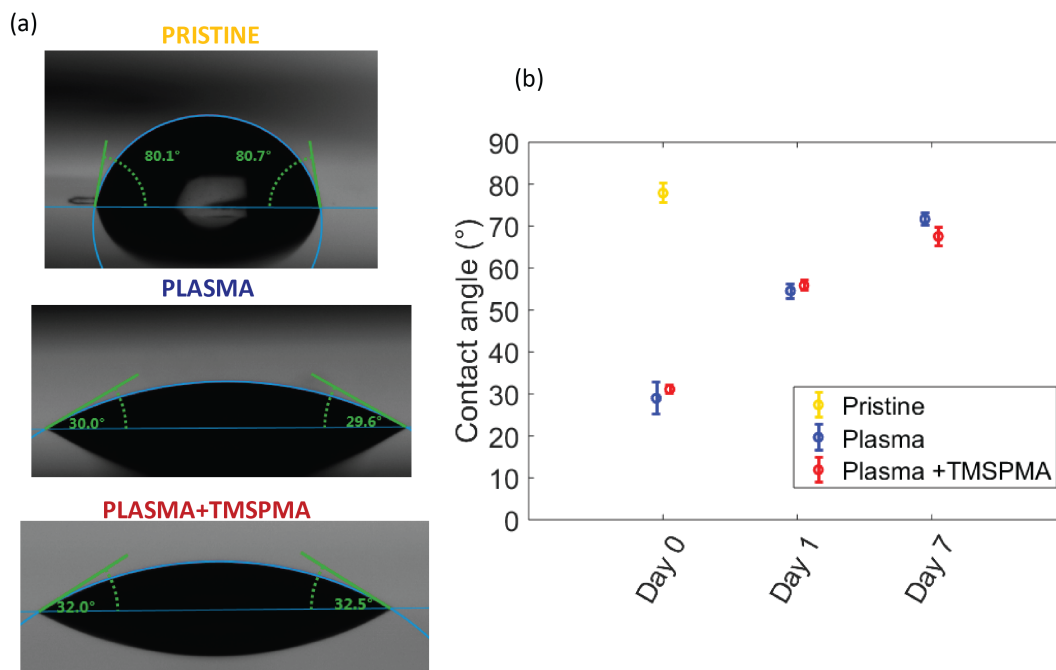


Figure 4.3 – **Contact angle measurements of pristine and treated PI samples.** Images of water drops on plain and treated PI surfaces, with corresponding contact angles, immediately after treatment (a), variation of contact angle at 24 hours and 7 days from initial treatment (b). Data presented as mean  $\pm$  std deviation (n=4).

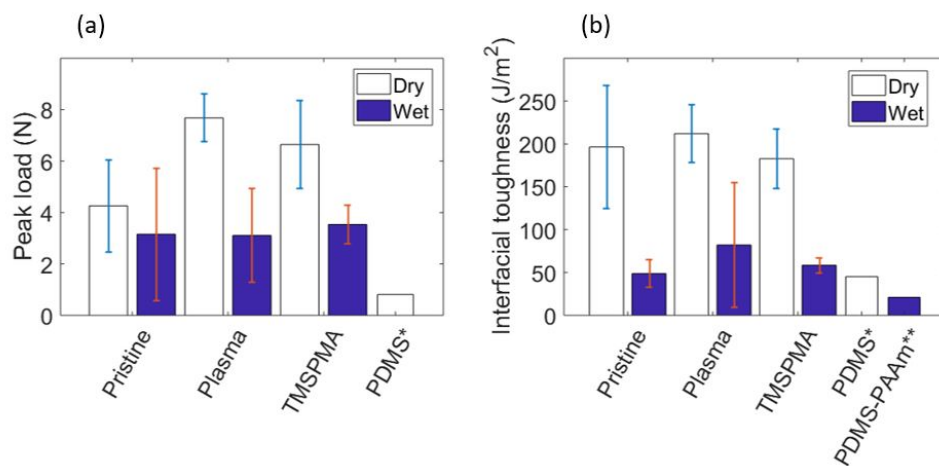


Figure 4.4 – **T-peel test results for PI layers bonded by PHEMA hydrogel.** Peak load (a) and interfacial toughness (expressed as average load over sample width) (b) for pristine and treated (plasma, plasma+TMSPMA) PI samples, both in the wet and dry state of the hydrogel (b). \*Plasma-bonded-PDMS. \*\*Bonded PDMS and PAAm in a 90° peel test [53]. Data presented as mean  $\pm$  std deviation (n=4).

No statistically significant difference (one-way ANOVA p value  $< 0.05$  deemed significant) was found between treatments, with the exception of plasma treated samples in the dry state compared to pristine samples ( $p = 0.028$ ). Overall the initial force required

in all configurations was still higher than plasma-bonded PDMS (0.8 N).

Interfacial toughness exhibited a comparable behavior, with no significant difference between treatments and a generally lower peel strength in the wet state: values varied from 197 J/m<sup>2</sup> to 49 J/m<sup>2</sup> for pristine samples, from 212 J/m<sup>2</sup> to 82 J/m<sup>2</sup> for plasma, from 183 J/m<sup>2</sup> to 59 J/m<sup>2</sup> for TMSPMA (fig. 4.4b). Again, all considered configurations showed improved values of interfacial toughness compared to PDMS (45 J/m<sup>2</sup>) and the PDMS-PAAm system (21 J/m<sup>2</sup>).

Accelerated aging of PI-PHEMA bilayers at 55 °C in PBS for 1 month resulted in delamination of the hydrogel from the underlying layer and appearance of cracks on its top surface, which was not the case for treated samples (fig. 4.5b).

The weight percent variation  $w\% = \frac{|w_f - w_i|}{w_i} \cdot 100$  of plasma-treated PI-PHEMA probes kept in agarose over 7 days was in the range of 1-2%, suggesting (for n=1) a lack of weight loss due to hydrogel delamination (fig. 4.5a).

Overall, the outcome of contact angle measurements, T-peel tests and accelerated aging tests showed no significant difference between plasma and plasma+TMSPMA, as both methods promoted surface wettability and showed no sign of degradation and delamination, as opposed to pristine samples. This led to the selection of O<sub>2</sub> plasma as a suitable polyimide surface treatment to promote the adhesion of PHEMA.

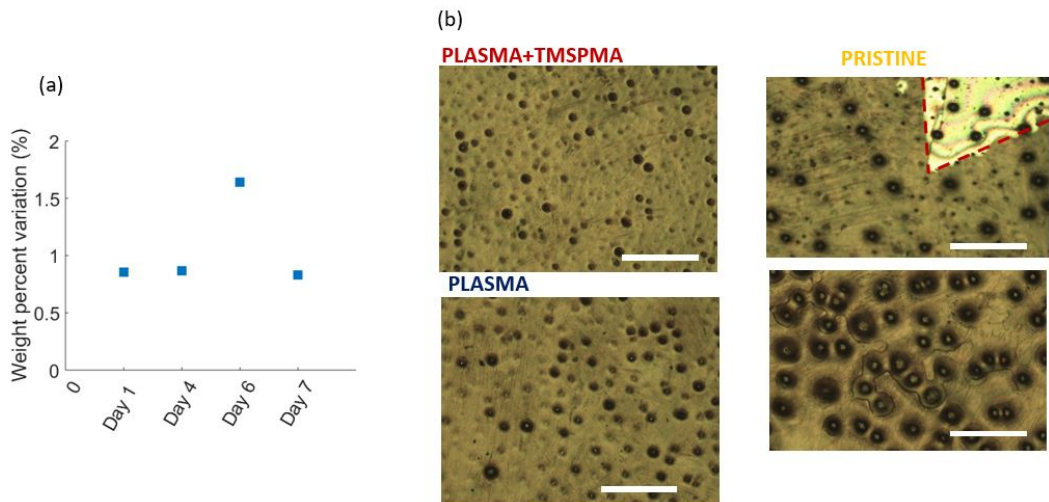


Figure 4.5 – **Accelerated aging of PI-PHEMA systems.** Weight percent variation of plasma-treated PI-PHEMA probes over 7 days (a), optical images of PHEMA on PI after 1 month in PBS at 55 °C for all 3 surface conditions (b). Scale bar 100  $\mu$ m.

#### 4.1.3 Buckling simulation

A 3D finite element analysis carried out with COMSOL Multiphysics 5.3 was used to predict mechanical buckling of multilayered (PHEMA-PDMS-PHEMA, PHEMA-PI-PHEMA) and plain PI probes. The first simulation of PHEMA-PDMS-PHEMA (120  $\mu$ m thickness) and PI (25  $\mu$ m thickness) probes with varying width ( $w = 100 \mu$ m, 200  $\mu$ m, 300  $\mu$ m) demonstrated an accurate prediction of probe insertion *in vivo* and in agarose models (fig. 4.6a-b). Successful insertion was observed only for probes with a 300  $\mu$ m width, with a critical buckling load above 1000  $\mu$ N. Values in and below the insertion force range (500-1000  $\mu$ N) were associated with a failed insertion, thus only the upper limit of the range was considered for later simulations.

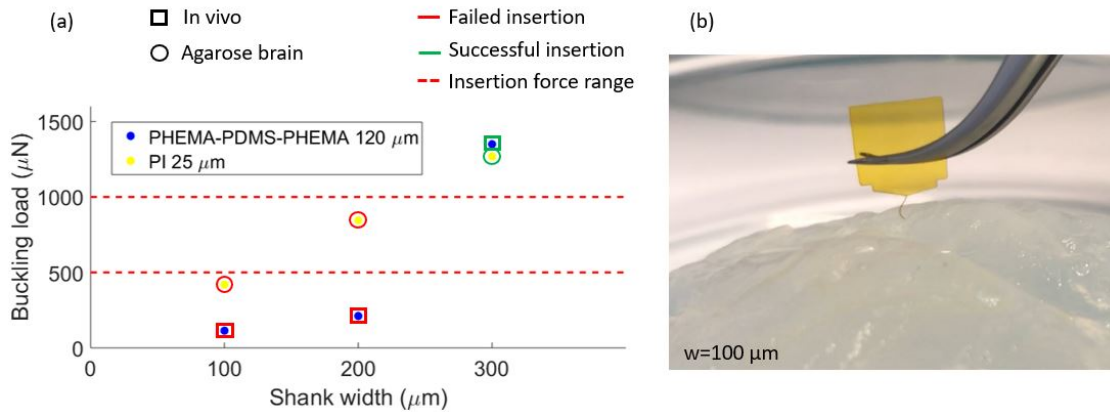


Figure 4.6 – **Simulation and experimental testing of probe buckling.** Comparison of simulation outcomes with insertion tests of PI probe in agarose and PHEMA-PDMS-PHEMA probes *in vivo* (a), example of PI probe ( $t = 25 \mu\text{m}$ ,  $w = 100 \mu\text{m}$ ) buckling upon insertion in agarose brain (b).

The second simulation led to the selection of an adequate coating thickness to ensure successful insertion of a PHEMA-PI-PHEMA configuration. Values of hydrogel coating, which were swept from  $2 \mu\text{m}$  to  $20 \mu\text{m}$  with a  $2 \mu\text{m}$  step, all resulted in a critical buckling load over  $1000 \mu\text{N}$ , with the exception of the  $2 \mu\text{m}$  coating ( $838 \mu\text{N}$ ) (fig. 4.7). A significantly high buckling load was observed for the  $20 \mu\text{m}$  thickness ( $52.8 \text{ mN}$ ).

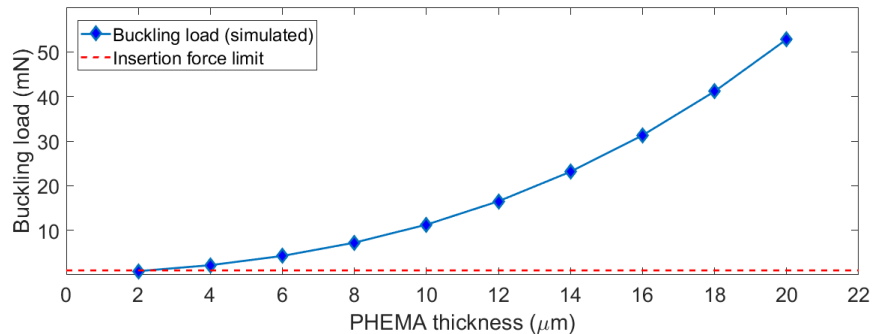


Figure 4.7 – **Buckling simulation of PHEMA-PI-PHEMA probes with different coating thickness.** Buckling load vs. PHEMA coating thickness on each side of PHEMA-PI-PHEMA probes, with coating varying from  $2 \mu\text{m}$  to  $20 \mu\text{m}$ , compared to an insertion force limit of  $1 \text{ mN}$ .

As a result of the simulation, the  $20 \mu\text{m}$  coating thickness was selected for the proposed probe. The overall thickness of the device ( $50 \mu\text{m}$ ) represents a 2x reduction compared to the PHEMA-PDMS-PHEMA model currently used within the research group and is comparable to commercial devices such as NeuroNexus probes.

#### 4.1.4 Passive probe fabrication

The process described in section 3.2.5 was used to fabricate passive hydrogel-encapsulated polyimide probes. The overall thickness of the obtained devices varied from  $50\ \mu\text{m}$  to  $60\ \mu\text{m}$ , due to variability in hydrogel thickness. Slightly asymmetrical coatings were thus observed in all samples (fig. 4.8a). Laser cutting of the fabricated devices resulted in limited resolution, with shank width varying in a range between  $320\ \mu\text{m}$  and  $330\ \mu\text{m}$  instead of the nominal  $300\ \mu\text{m}$  (fig. 4.8b). All prepared devices were successfully and easily inserted in agarose brain.

Despite all precautions taken to maintain probes flat, curling of the asymmetrical PHEMA-PI-PHEMA probes was observed in the high-humidity environment of the surgery room (fig. 4.8c). This was most probably due to the different stresses acting on each PI side and due to the quick rehydration of the thin hydrogel layers.

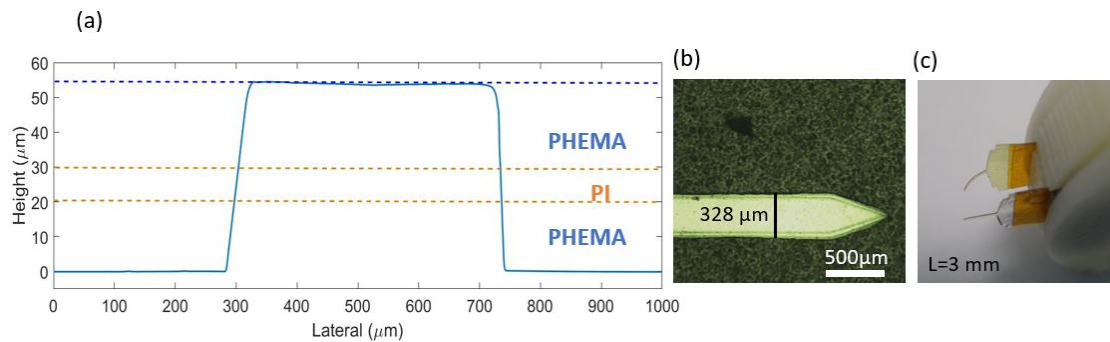


Figure 4.8 – **Fabricated passive probes** Asymmetrical hydrogel coating on each side observed through mechanical profilometry (a), optical image of laser cut probe with  $328\ \mu\text{m}$  width (b), curling of PHEMA-PI-PHEMA probe (top), compared to symmetric PHEMA-PDMS-PHEMA probe (bottom) in humid surgical conditions (c).

#### 4.1.5 *In vivo* study results

Despite curling due to surgery-related high humidity, one probe was successfully inserted, while the second appeared to have an uncertain outcome. For this reason, only tissue from the first rat was processed and analyzed. Images were analyzed qualitatively, as only one sample was taken into consideration.

Microscope images of successive  $40\ \mu\text{m}$  slices further illustrated probe curling after insertion (fig. 4.9a). By overlapping successive images it was possible to visualize the probe shape and estimate the depth of insertion of the probe ( $580\ \mu\text{m}$ ) (fig. 4.9d).

Immunolabeled fluorescent images of the insertion site were compared to control images taken from undamaged areas of the brain. NeuN staining highlighted the presence of neurons in close proximity to the probe, while GFAP staining illustrated astrocytic scarring just surrounding the implant and in the upper area corresponding to the location of the craniotomy (fig. 4.9b), which is naturally more subject to scarring. Iba1 staining demonstrated a low immune response: a small quantity of activated microglia, represented by the larger cell bodies around the implant, was observed (fig. 4.9c).

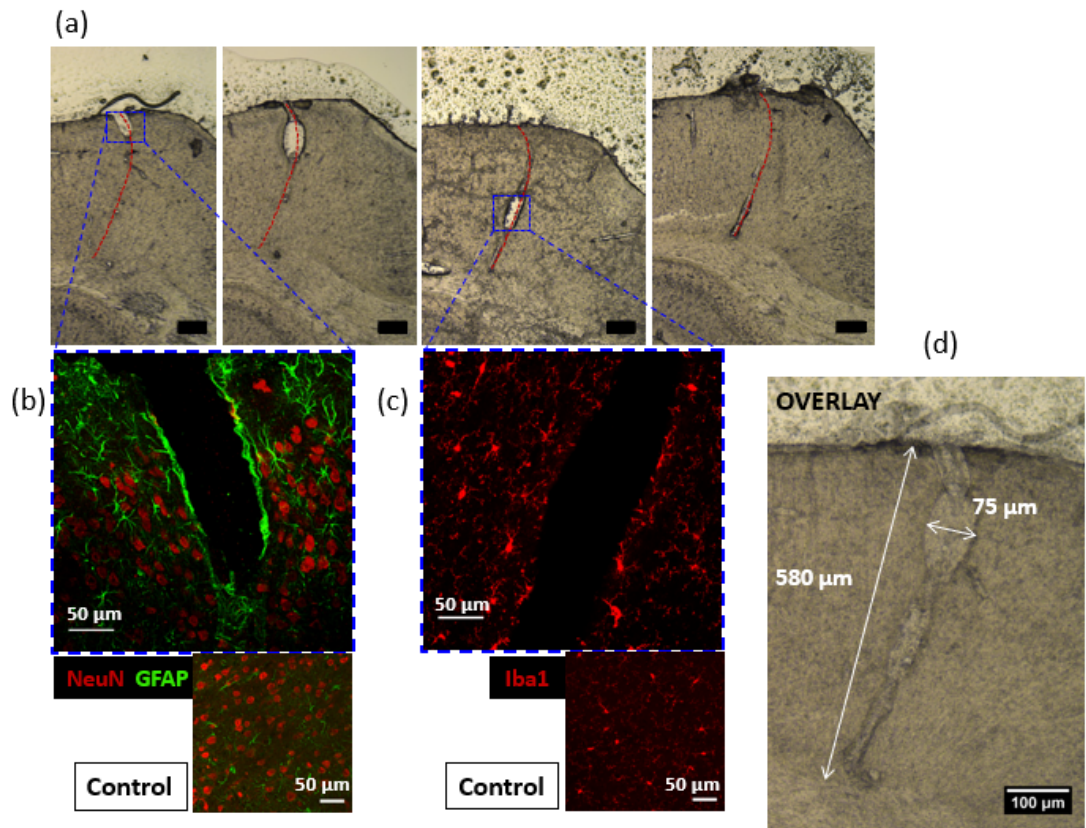


Figure 4.9 – **Tissue reaction surrounding implant site.** Microscope images of implant site on successive 40  $\mu\text{m}$  slices (scale bar 100  $\mu\text{m}$ ) (a). Insets: representative images of immunolabeled tissue showing presence of neuronal nuclei (NeuN), astrocytic scar (GFAP) (b) and microglia immune response (Iba1) (c), overlay of microscope images defining probe shape and estimated insertion depth (d).

GFAP staining was then compared for PHEMA-PI-PHEMA ( $t_{dry} = 50 \mu\text{m}$ ) (fig. 4.10a), PHEMA-PDMS-PHEMA ( $t_{dry} = 125 \mu\text{m}$ ) (fig. 4.10b) and silicon ( $t = 125 \mu\text{m}$ ) (fig. 4.10c) probes. Scarring surrounding the PI-based probe suggests a deeper penetration of implants, which appeared to be bent within the cortex after approximately 500  $\mu\text{m}$  of insertion. Soft PHEMA-coated implants showed a similar tissue reaction, with observable scarring just surrounding the insertion site, while a stiff silicon reference showed a much broader scar, all along the length of the shank. Furthermore, a wide opening was observable only for the silicon probe, illustrating the damage undergone by brain tissue during implant removal. Due to a significant implant encapsulation, a large quantity of tissue was removed, an issue which did not occur for soft probes, which presented openings comparable to actual implant thickness.

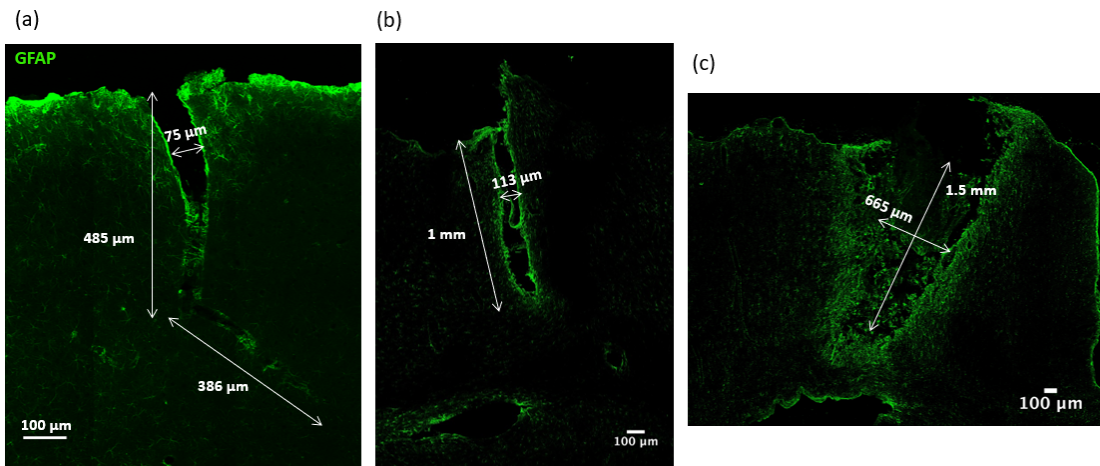


Figure 4.10 – **Comparison of GFAP staining on soft and stiff implants.** Astrocytic scar around PHEMA-PI-PHEMA ( $t_{dry} = 50 \mu\text{m}$ ) (a), PHEMA-PDMS-PHEMA ( $t_{dry} = 125 \mu\text{m}$ ) (b) and silicon ( $t = 125 \mu\text{m}$ ) (c) probes.

## 4.2 Electroactive probes

### 4.2.1 Probe fabrication and characterization

By employing the standard process described in section 3.3.2 uniform and undamaged Pt electrodes and tracks were sputtered, etched and encapsulated in PI (fig. 4.11). Successive etching of polyimide and spin coating of hydrogel were performed resulting in no noticeable damage to the underlying structures.

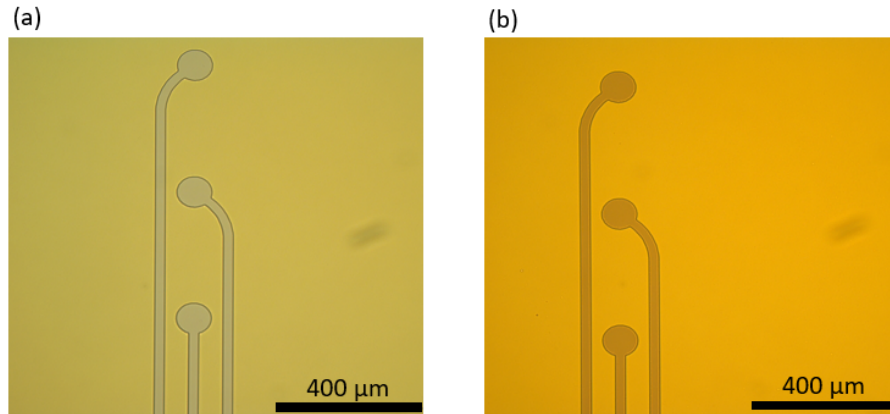


Figure 4.11 – **PI/Pt/PI encapsulation.** Optical microscopy images of Pt tracks and electrodes sputtered and etched on the PI layer (a), Pt encapsulated between two layers of PI (b).

The etching of hydrogel, performed using underdeveloped photoresist as a mask, however, produced significantly different results based on the technique used to expose the photoresist. In the case of uniformly exposed photoresist ( $340 \text{ mJ/cm}^2$ ), different feature sizes developed at different rates resulting in different photoresist thicknesses covering pads and contacts. Specifically, the development over small contacts ( $\varnothing = 100 \mu\text{m}$ ) was faster compared to the pads ( $2 \text{ mm} \times 1 \text{ mm}$ ). As a consequence, a shorter etching time was required to open the contacts. Successive  $\text{O}_2$  etching, required to remove the remaining hydrogel from Pt pads, resulted in significant damage to the already-exposed contacts.

SEM imaging allowed the investigation of the morphology of Pt on the two different types of features. Contacts appeared to be damaged, with granular debris around their borders (fig. 4.12a), whereas the surface of pads was uniform and intact (fig. 4.12b). EDS analysis was performed to verify the elemental composition of the sample. As expected, platinum was not detected along the center of the contact (fig. 4.13a), suggesting that the additional plasma etching (1-2 min) had in fact physically removed the metal and exposed the first organic polyimide layer. On the contrary, platinum was uniformly detected along large pads (fig. 4.13b).

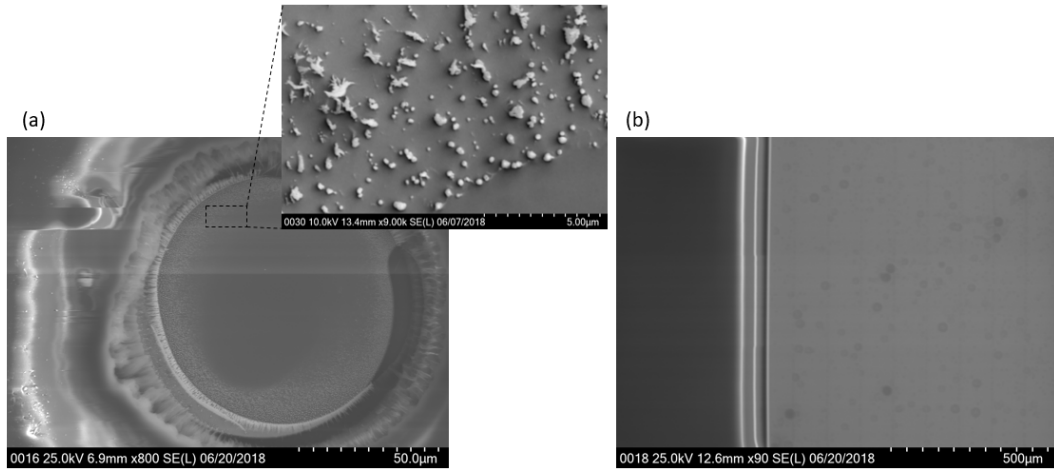


Figure 4.12 – **SEM images of open electrodes and pads (same exposure dose).** Electrode which has undergone excessive etching presents residual Pt only at the edges, inset shows residual debris of Pt (a). Uniform Pt surface across pad (b).

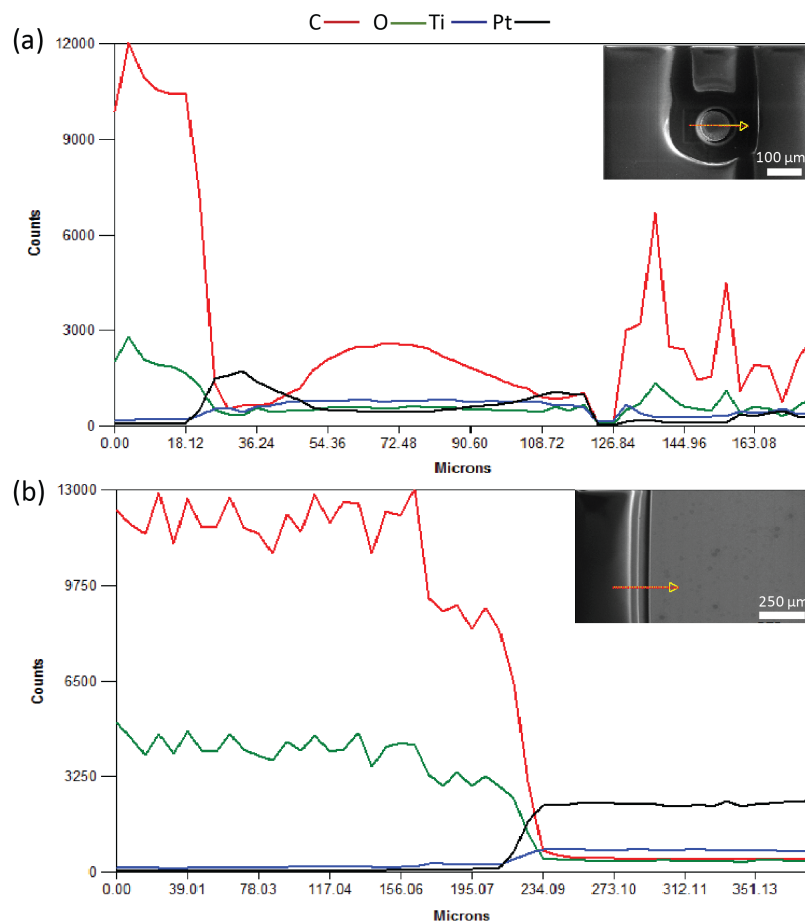


Figure 4.13 – **EDS analysis of electrodes and pads (same exposure dose).** Linescan of damaged electrode illustrating absence of Pt around the center of the contact (a), linescan over pad illustrating Pt uniformity (b).

Based on these results, a different exposure dose was used for small contacts and it was optimized in order to obtain a comparable photoresist step (approximately 14  $\mu\text{m}$ ) on both features (fig. 4.14). Using this technique led to a significant improvement, with both electrodes and pads resulting undamaged (fig. 4.15). EDS analysis also detected a stable layer of Pt on both features (fig. 4.16).

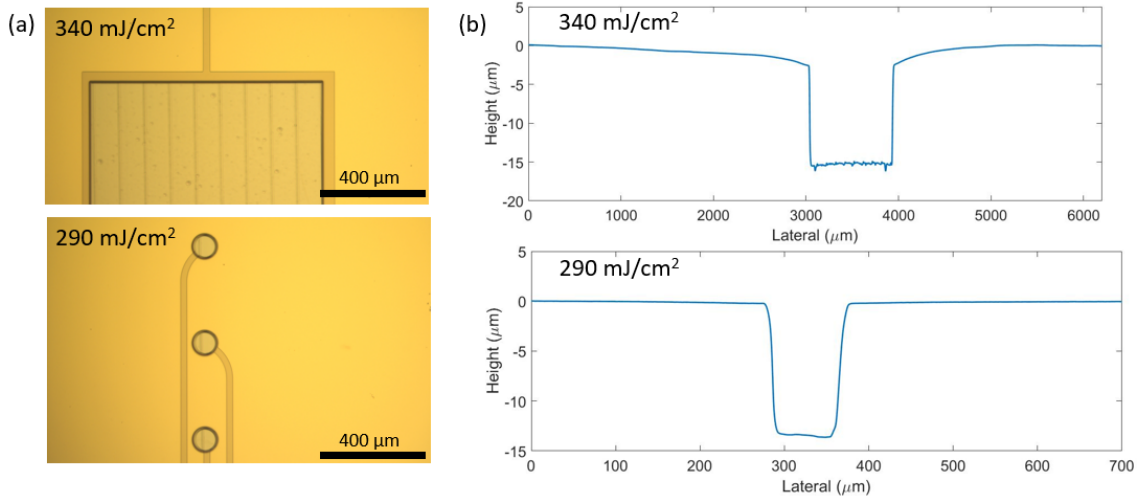


Figure 4.14 – **Photoresist underdevelopment on electrodes and pads.** Microscope images of desired residual resist (a), profile of similar resist step over contacts and pads (b).

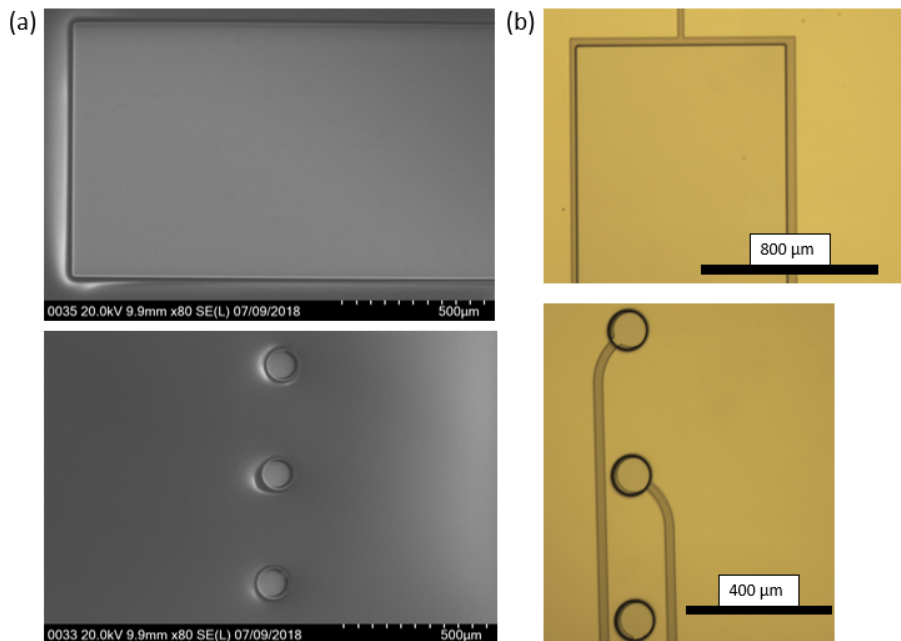


Figure 4.15 – **Open electrodes and pads (different exposure dose).** SEM images (a) and optical microscopy images (b) of undamaged and uniform Pt pads and electrodes.

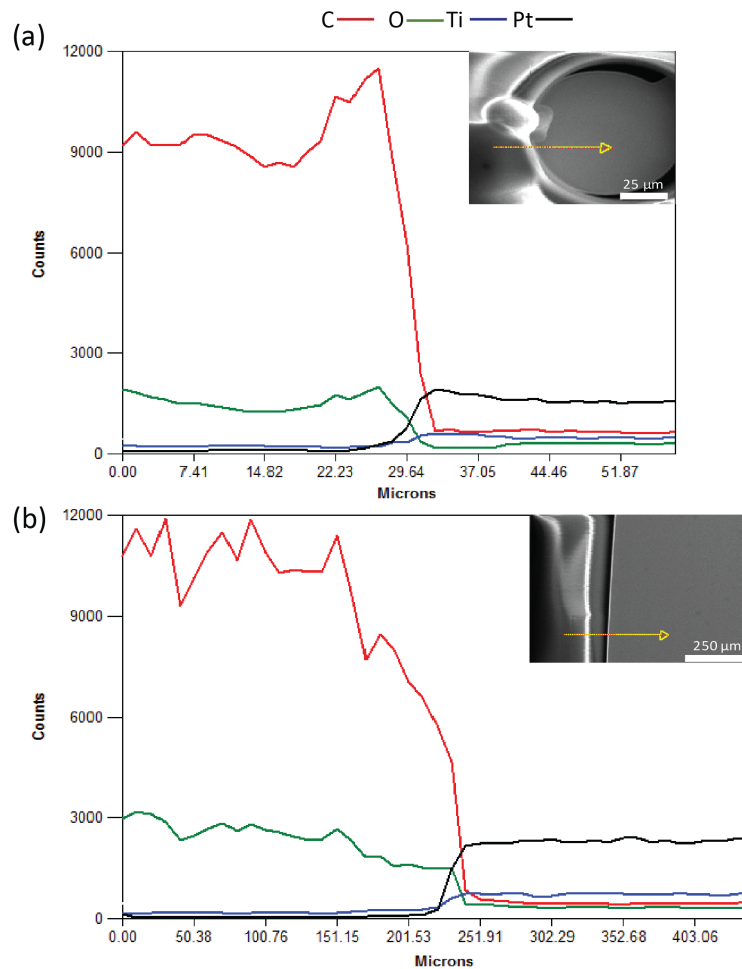


Figure 4.16 – **EDS analysis of electrodes and pads (different exposure dose).** Linescan over electrode (a) and pad (b) illustrating a uniform layer of platinum.

In the last steps of the process polyimide was released from the carrier wafer either manually or through an anodic release. While the integrity of the Pt electrodes and tracks was maintained in both cases, the hydrogel layer remained unchanged only with the dry release (fig. 4.17a). The hydration and dehydration undergone by the hydrogel layer determined the appearance of surface irregularities and misalignment of different entity across the entire wafer (fig. 4.17b).

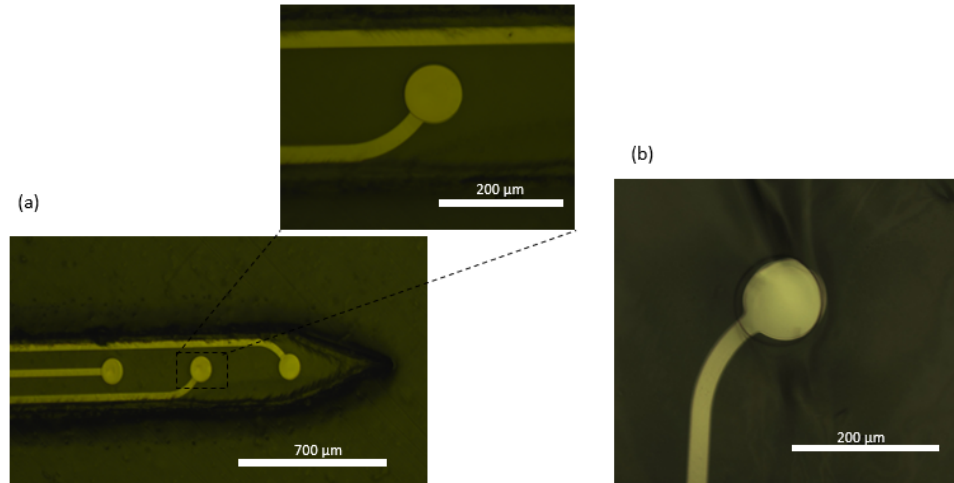


Figure 4.17 – **Dry release vs. anodic release of polyimide.** Optical microscopy images of a dry-released probe with no hydrogel alteration (a) and slightly damaged and misaligned hydrogel over an anodically-released probe (b).

#### 4.2.2 Preliminary *in vitro* and *in vivo* results

Preliminary tests performed on the anodically-released probes were not successful. A first *in vivo* recording attempt did not register any neural activity in response to sciatic nerve and optical stimulation, but did register stimulation artifacts. Electrochemical tests were inconclusive and in all cases an impedance in the order of  $1\text{ M}\Omega$  ( $f = 1\text{ kHz}$ ) was found. It is unclear whether this was due to issues with the electrodes themselves or with the wiring process. CV and impedance measurements were later repeated on the dry-released probes. At  $1\text{ kHz}$  the recorded impedance (fig. 4.18a) was  $69.64\text{ k}\Omega \pm 18.56\text{ k}\Omega$  ( $n=6$ ), significantly lower than the previous attempts. Measured currents were found to be below the order of  $\mu\text{A}$  (fig. 4.18b), generally ranging between  $-300\text{ nA}$  and  $300\text{ nA}$ . CV curve shapes differed from one electrode to the other, suggesting a variability related either to the electrodes or the connectors.

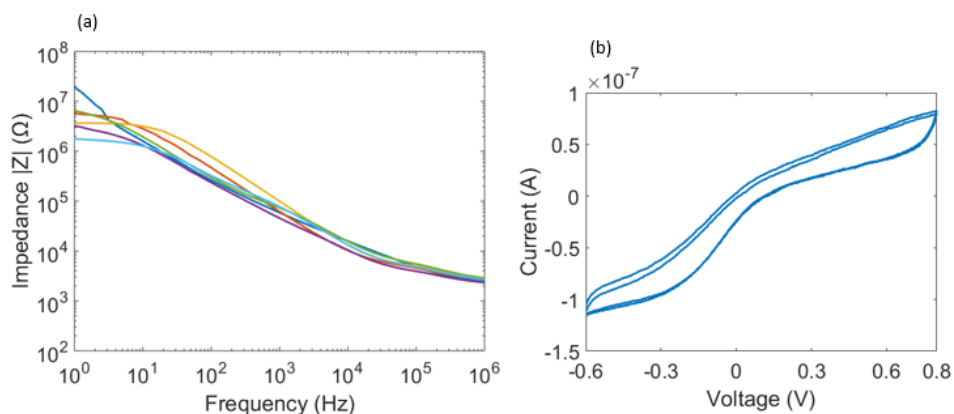


Figure 4.18 – **Electrochemical characterization of Pt electrodes** ( $\varnothing = 100\text{ }\mu\text{m}$ ). Impedance spectroscopy of bare Pt electrodes ( $n=6$ ) (a) and an example of CV curve for one electrode (2nd and 3rd cycle) (b).

## 5 Discussion

This study was proposed to investigate the effect of a PHEMA hydrogel coating on a flexible polyimide neural implant in terms of brain tissue reaction, and to assess the feasibility of developing a functional recording implant integrating these materials. An essential feature of the used hydrogel is related to its tunable mechanical properties, which were quantified during previous studies. The formulation employed in fact guarantees a wide variation of the Young's modulus: from 8-9 GPa in the dry state to 220 kPa in the wet state. This allows the coating to be sufficiently stiff during the implantation phase, favoring a successful insertion and, at the same time, to be soft enough after implantation, to shield the brain tissue from the stiff substrate materials. The other favorable feature of the hydrogel is its relatively limited swelling: a 27% increase in volume is generally observed in hydrated conditions, which is significantly lower than the 300% increase reported for alginate [38]. Ongoing studies are currently assessing the beneficial effect of the PHEMA coating on PDMS passive probes under acute and chronic conditions. In the context of this project, polyimide was chosen as a substrate to ease the transition towards the development of an active probe, as it presents a more standard integration of metal electrodes.

The PI-PHEMA material combination was evaluated from a mechanical point of view and the observed behavior further justified the choice. In terms of conformability, single materials performed as predicted, with low Young's modulus materials (PHEMA, PDMS) easily folding onto underlying cylindrical and spherical structures, consistently with theoretical equations (fig. 4.1). In the considered range of curvature radii (2-4 mm), softer films with thicknesses up to few hundreds of microns could conform, whereas plain polyimide samples required thicknesses one order of magnitude lower. However, when dealing with a PI thickness of 10  $\mu\text{m}$  encapsulated in hydrogel, the system exhibited a conformability superior to that of plain PDMS, ensuring better contact and less damage to neural tissue.

A suitable method to properly integrate the two materials in the proposed multilayer system was found using plasma activation. Contact angle measurements confirmed an increased hydrophilicity for treated PI samples (fig. 4.3) and values found were consistent with those reported by Kondo *et al.* [54]. Their work also highlighted the surface roughness of PI after plasma activation, a feature which is typically associated with an improved adhesion. A successive TMSPMA hydrophilic silanization did not appear to alter the effects of a simple plasma activation, with both treatments exhibiting similar outcomes in all performed tests. A decrease in wettability was observed with angles varying in a range between 30° and 70° over 7 days and accelerated aging demonstrated lower degradation for treated samples. T-peel test results, expressed in terms of peak load and interfacial toughness (fig. 4.4), were somewhat unexpected, showing no significant difference between pristine and treated samples in the wet state. Nevertheless, a significant improvement was observed due to plasma activation on dry samples, a desirable outcome to favor integrity and avoid delamination due to shear forces during the dry implantation phase. Given the limited differences between treatments, an analysis of chemical surface modification could be carried out to better comprehend the grafting mechanisms.

The complete multilayer probe was fabricated using a 20  $\mu\text{m}$  coating thickness on each side, as a result of the COMSOL buckling simulation (fig. 4.7). A 52.8 mN critical buckling load was achieved, a value significantly higher than the 1 mN insertion force limit. In this configuration, the probe was much thinner than most hydrogel-coated implants reported in literature, which are in the order of hundreds of microns [18]. A critical issue

observed throughout the fabrication process was related to the dispensing of hydrogel. Its sensitivity to light and temperature determined variability in viscosity which translated to a variation in thickness. Furthermore, the adopted method did not allow for a perfectly symmetrical coating. A possible improvement could be obtained by performing a rheological study of PHEMA, to verify its properties prior to spin-coating. While all fabricated samples were easily inserted in phantom agarose brain, the implantation *in vivo* was hampered by the significant curling effect (fig. 4.8c) linked to coating asymmetry and surgical humidity conditions. As a consequence, probes were straightened and inserted slowly. The longer time required to implant probes may have also determined a further rehydration of the hydrogel; additionally, studies have shown that a faster penetration speed (1 mm/s) is preferable to obtain a successful insertion [55].

Tissue reaction after 7 days was evaluated qualitatively from immunofluorescent images. Results suggested a minimal damage occurring during the acute inflammation phase, with low neuronal loss and low scarring compared to stiff implants (fig.4.9-4.10). A 20  $\mu\text{m}$  coating appeared to be sufficient to properly shield the surrounding tissue from the stiffer polyimide substrate, which is in accordance with findings from Buxboim *et al.* [56], who reported that cells respond to the stiffness of underlying rigid materials, protected by gel layers, at a threshold gel thickness of 10-20  $\mu\text{m}$ . Due to the limited number of animals tested and the limited data available, a significant conclusion could not be drawn from these results. A further analysis is required to evaluate the effect of a thin coating over the short and long term. By performing a larger animal study, neuronal and astrocytocal densities could be statistically quantified and compared for different implant types. If confirmed, these results could be promising to obtain long-term stable recordings, as the reduced thickness and limited swelling shorten the distance between recording sites and target neurons; simultaneously, the low scarring observed limits the isolation and impedance increase.

Active probes incorporating Pt electrodes and coated with PHEMA were fabricated adapting a hydrogel patterning technique proposed by Lei *et al.* [42], based on the underdevelopment of photoresist to avoid hydrogel swelling and damage. The group reported very promising results, achieving a 2.5  $\mu\text{m}$  resolution. This, however, was obtained with 1.3  $\mu\text{m}$  thick hydrogels patterned in micron scale free-standing structures. The implementation of this method thus required a number of optimizations to obtain uniform results at the wafer-scale. Firstly, a dry stripping of photoresist was implemented, as the acetone removal proposed by Lei led to hydrogel cracking. Chemically, the oxygen treatment does not etch Pt, however the physical bombardment of plasma species on the metal surface determined noticeable damage and poor resolution even after 2-5 minutes of additional etching (fig. 5.1a). Minimizing residual resist solved etching issues only partially. Underdevelopment had to be carefully calibrated, as contact between developer and PHEMA resulted in cracking of hydrogel and of the underlying Pt and PI after etching (fig. 5.1b). Using optimized exposure doses (340  $\text{mJ}/\text{cm}^2$ , 290  $\text{mJ}/\text{cm}^2$ ) and development time (360 s), uniform results were obtained (fig. 4.15-4.16). Nevertheless, the applicability of this method is limited to relatively flat hydrogel surfaces. In fact, a thickness variation of more than 5  $\mu\text{m}$  over the different features to be patterned would result in at least 2 minutes of unnecessary etching of already-opened pads or contacts. In case of hydrogel thickness variability, exposure doses should be adapted to provide a disparity in the photoresist step over each feature type, thus balancing out the overall etching time.

The anodic release in NaCl solution of the patterned PI-PHEMA bilayer inevitably damaged the hydrogel layer. This, however, occurred to a lesser extent compared to the

effects of hydration/dehydration performed on wafer, as the underlying polyimide substrate allows for a higher degree of flexibility. The consequent misalignment (fig. 4.17b) rendered the electrodes inoperable in approximately 30 % of the cases, as they had been covered by the shifted PHEMA. In ongoing studies a dry release of the bilayer is being optimized. As expected, first results showed that there was no deterioration of the electrodes (fig. 4.17a). While this represents a positive preliminary result, a drawback of the proposed dry release method is related to the spontaneous delamination of polyimide from the edges of the wafer during standard microfabrication conditions, such as vacuum and wet steps.

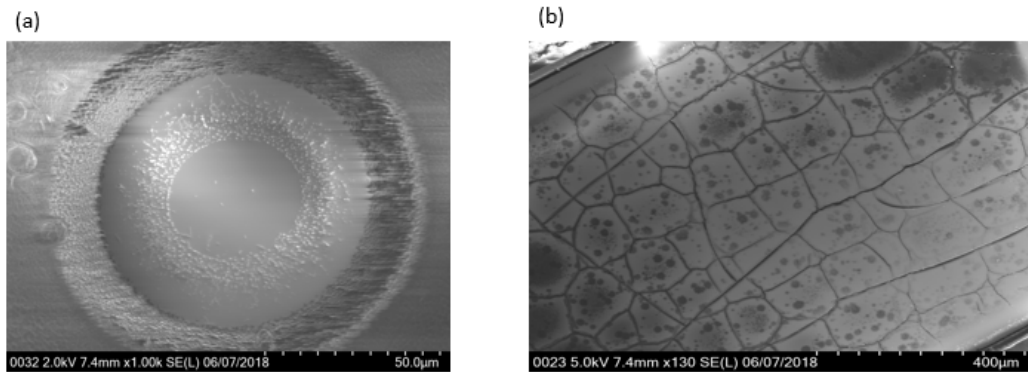


Figure 5.1 – **Consequences of excessive  $O_2$  etching of platinum.** SEM images of an overetched contact, resulting in removal of Pt and poor resolution (a) and an overetched pad, cracked due to the complete development of photoresist and the consequent damage and cracking of hydrogel (b).

First *in vivo* and *in vitro* tests were not successful, with no neural activity recorded and  $1\text{ M}\Omega$  impedances observed for  $100\text{ }\mu\text{m}$  diameter Pt electrodes. Successive electrochemical characterization performed on dry-released probes with a different connector configuration (fig. 5.2c) yielded a  $69.64\text{ k}\Omega \pm 18.56\text{ k}\Omega$  impedance at  $1\text{ kHz}$  and currents in the range of few hundreds of nA. Considering the large area of the contact, the obtained values were still not optimal, yet plausible for a bare sputtered platinum electrodes and comparable to values reported by Guex *et al.* ( $45.27\text{ k}\Omega \pm 2.62\text{ k}\Omega$ ) [57]. Low detected currents could be associated with connector or track-related issues.

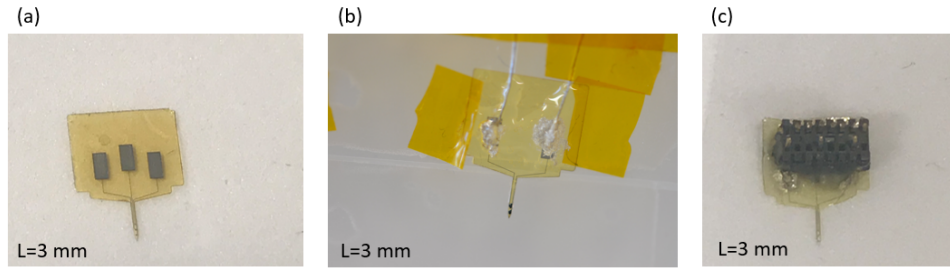


Figure 5.2 – **Fabricated active probes and electrical connections.** Laser cut active probe (a), electrical connections established with silver paste and wires (b) or mounting a connector over the electrode pads (c).

The data and preliminary results presented here support the idea of implementing a hydrogel-coated polyimide intracortical probe for long-term neural recording and stimulation. To achieve this goal it is essential that in future work the hydrogel dispensing be optimized to ensure a symmetrical coating and also an overall reduced variability, to avoid any inhomogeneities during successive patterning steps. Additionally, further work is required to perfection the establishment of electrical connections. These improvements would allow the development of flat, implantable and functional probes in a more reliable and repeatable manner.

## 6 Conclusions

In this work an intracortical probe combining the beneficial effects of mechanically-compliant materials and of a reduced geometrical footprint was proposed. A thin and soft poly(2-hydroxyethyl methacrylate)-polyimide implant was designed, fabricated, characterized and tested *in vivo*. The integration of the hydrogel and the flexible substrate was evaluated and it was shown that PI can maintain a long-term stable grafting with PHEMA, generating a highly conformable system. The hydrogel proved to act as a rigid backbone in the dry state ( $E \approx 8$  GPa) promoting device insertion, as demonstrated by finite element modeling and experimental penetration tests. After implantation, PHEMA behaved as a soft buffer layer ( $E \approx 220$  kPa) in the swollen state, reducing adverse tissue reaction. Short-term (7 days) *in vivo* tests were promising and highlighted minimal scarring, inflammation and neuronal loss, despite the limited hydrogel coating thickness (20  $\mu\text{m}$ ). Nevertheless, experiments led to the identification of a critical issue in the fabrication of the multilayered devices, due to the variability in hydrogel dispensing. The generation of coatings was asymmetrical: it determined a curling effect and compromised device insertion, thus requiring further optimization.

By underdeveloping photoresist, standard photolithography was used to pattern PHEMA, without altering or damaging the hydrogel itself, which is naturally sensitive to environmental changes. The fabrication method proposed was successful in patterning 20  $\mu\text{m}$  thick structures, but it could be, in principle, applicable to different thicknesses and feature sizes, by properly calibrating exposure dose and development time of the photoresist mask. The combined integration of hydrogel as a coating and Pt as electrode material, encapsulated between polyimide layers, made the overall system applicable to *in vivo* recording. Even though preliminary *in vivo* tests did not detect neural activity, impedance characterization of successively fabricated devices with bare Pt electrodes appeared to be promising and suggested device functionality ( $69.64 \text{ k}\Omega \pm 18.56 \text{ k}\Omega$  impedance modulus at 1 kHz).

Overall, the conducted experiments provided a preliminary confirmation of the positive effect of a thin hydrogel coating on a polyimide probe, in relation to foreign body reaction. Furthermore, a proof-of-concept method for the development of active probes was demonstrated, highlighting the importance and the challenges associated with maintaining the hydrogel in a dehydrated state throughout all fabrication steps. The outcome of this work thus represents a first promising step towards the achievement of a stable long-term investigation and stimulation of the central nervous system.

### 6.1 Outlook

Current work includes the optimization of a completely dry fabrication process, the development of strategies to ensure a symmetrical coating and prevent shank curling, and the identification of a technique to properly deposit the soft PEDOT:PSS composite over the Pt recording sites, to lower electrode impedance. In order to confirm preliminary results presented in this work, a further *in vivo* investigation would be required in both acute and chronic settings, to evaluate tissue response and the ability to record neural activity. In the overall context of the project, one long-term goal consists in the transition from a single shank device to a 2D system in the Utah array configuration, to exploit a higher number of recording sites and locations. Finally, the device could be further optimized by implementing the fabrication of micro-cracked PI/Pt/PI, a structure developed at the LSBI, to also promote stretchability of the implant, aside from the already-confirmed softness and flexibility.

## List of Figures

1.1	Mechanical mismatch between stiff implants and soft tissue. . . . .	2
1.2	Schematic comparison of tissue response around stiff (A) and compliant (B) probes. . . . .	3
2.1	Schematic illustration of fabrication steps for parylene neural probes. . . .	4
2.2	E-dura implant, with SEM inserts of interconnects and electrodes. . . . .	5
2.3	Reswelling of alginate coating on silicon probes in agar. . . . .	7
3.1	Molecular structure of poly(2-hydroxyethyl methacrylate) . . . . .	8
3.2	Conformability of different thicknesses of PHEMA, PDMS and PI. . . . .	9
3.3	Conformability of a polyimide layer encapsulated in PHEMA. . . . .	10
3.4	T-peel test for PI-PHEMA samples. . . . .	12
3.5	Schematic illustration of passive probe design. . . . .	13
3.6	Schematic illustration of simulated probes. . . . .	14
3.7	Process flow for PI release and hydrogel encapsulation. . . . .	16
3.8	Surgical procedure for probe implantation. . . . .	17
3.9	Schematic illustration of electroactive probe. . . . .	18
3.10	Process flow for PI/Pt/PI stack. . . . .	19
3.11	Methods for hydrogel etching. . . . .	20
3.12	Process flow for encapsulation in hydrogel of PI/Pt/PI stack. . . . .	21
3.13	Dry process flow for the fabrication of active probes. . . . .	22
4.1	Experimental conformability of PHEMA, PI and PDMS. . . . .	24
4.2	Theoretical and experimental conformability of PHEMA-PI-PHEMA. . . .	25
4.3	Contact angle measurements of pristine and treated PI samples. . . . .	26
4.4	T-peel test results for PI layers bonded by PHEMA hydrogel. . . . .	26
4.5	Accelerated aging of PI-PHEMA systems. . . . .	27
4.6	Simulation and experimental testing of probe buckling. . . . .	28
4.7	Buckling simulation of PHEMA-PI-PHEMA probes with different coating thickness. . . . .	28
4.8	Fabricated passive probes. . . . .	29
4.9	Tissue reaction surrounding implant site. . . . .	30
4.10	Comparison of GFAP staining on soft and stiff implants. . . . .	31
4.11	PI/Pt/PI encapsulation. . . . .	32
4.12	SEM images of open electrodes and pads (same exposure dose). . . . .	33
4.13	EDS analysis of electrodes and pads (same exposure dose). . . . .	33
4.14	Photoresist underdevelopment on electrodes and pads. . . . .	34
4.15	Open electrodes and pads (different exposure dose). . . . .	34
4.16	EDS analysis of electrodes and pads (different exposure dose). . . . .	35
4.17	Dry release vs. anodic release of polyimide. . . . .	36
4.18	Electrochemical characterization of Pt electrodes ( $\varnothing = 100 \mu\text{m}$ ). . . . .	36
5.1	Consequences of excessive $\text{O}_2$ etching of platinum. . . . .	39
5.2	Fabricated active probes and electrical connections. . . . .	40

## List of Tables

1	Material properties used in finite element model. . . . .	14
---	---	----

## References

- [1] Y. Son, H. Jenny Lee, J. Kim, H. Shin, N. Choi, C. Justin Lee, E. S. Yoon, E. Yoon, K. D. Wise, T. Geun Kim, and I. J. Cho. In vivo optical modulation of neural signals using monolithically integrated two-dimensional neural probe arrays. *Scientific Reports*, 5(January):1–11, 2015.
- [2] J. P. Roche and M. R. Hansen. On the Horizon: Cochlear implant technology. *Otoralyngologic Clinics of North America*, 48(6):1097–1116, 2015.
- [3] C. Fukaya and T. Yamamoto. Deep Brain Stimulation for Parkinson’s Disease: Recent Trends and Future Direction. *Neurologia medico-chirurgica*, 55(5):422–431, 2015.
- [4] M. S. Humayun, J. D. Weiland, G. Y. Fujii, R. Greenberg, R. Williamson, J. Little, B. Mech, V. Cimarusti, G. Van Boemel, G. Dagnelie, and E. De Juan. Visual perception in a blind subject with a chronic microelectronic retinal prosthesis. *Vision Research*, 43(24):2573–2581, 2003.
- [5] D. O. Adewole, M. D. Serruya, J. P Harris, J. C Burrell, H. I. Chen, J. A Wolf, D. K. Cullen, and M. J. Crescenz. The Evolution of Neuroprosthetic Interfaces. *Critical Reviews in Biomedical Engineering*, 44(1-2):123–152, 2017.
- [6] M. Jorfi, J. L. Skousen, C. Weder, and J. R. Capadona. Progress towards biocompatible intracortical microelectrodes for neural interfacing applications. *Journal of Neural Engineering*, 12(1), 2015.
- [7] J. L. Collinger, B. Wodlinger, J. E. Downey, W. Wang, E. C. Tyler-Kabara, D. J. Weber, A. J.C. McMorland, M. Velliste, M. L. Boninger, and A. B. Schwartz. High-performance neuroprosthetic control by an individual with tetraplegia. *The Lancet*, 381(9866):557–564, 2013.
- [8] J. Wolpaw and E.W. Wolpaw. *Brain-Computer Interfaces: Principles and Practice*. Oxford University Press, USA, 2012.
- [9] I. Lazarou, S. Nikolopoulos, P. C. Petrantonakis, I. Kompatsiaris, and M. Tsolaki. EEG-Based Brain–Computer Interfaces for Communication and Rehabilitation of People with Motor Impairment: A Novel Approach of the 21st Century. *Frontiers in Human Neuroscience*, 12(January):1–18, 2018.
- [10] F. Ben Taher, N. Ben Amor, and M. Jallouli. EEG control of an electric wheelchair for disabled persons. *2013 International Conference on Individual and Collective Behaviors in Robotics - Proceedings of ICBR 2013*, pages 27–32, 2013.
- [11] T. Yang, S. Hakimian, and T. H. Schwartz. Intraoperative electroCorticoGraphy (ECog): Indications, techniques, and utility in epilepsy surgery. *Epileptic Disorders*, 16(3):271–279, 2014.
- [12] A. L. Benabid. Deep brain stimulation for Parkinson’s disease. *Current Opinion in Neurobiology*, 13(6):696–706, 2003.
- [13] E. Fernández, B. Greger, P. A. House, I. Aranda, C. Botella, J. Albusua, C. Soto-Sánchez, A. Alfaro, and R. A. Normann. Acute human brain responses to intracortical microelectrode arrays: challenges and future prospects. *Frontiers in Neuro-engineering*, 7(July):1–6, 2014.

- [14] C. M. Lopez, A. Andrei, S. Mitra, M. Welkenhuysen, W. Eberle, C. Bartic, R. Puers, R. F. Yazicioglu, and G. G.E. Gielen. An implantable 455-active-electrode 52-channel CMOS neural probe. *IEEE Journal of Solid-State Circuits*, 49(1):248–261, 2014.
- [15] J. C. Barrese, N. Rao, K. Paroo, C. Triebwasser, C. Vargas-Irwin, L. Franquemont, and J. P. Donoghue. Failure mode analysis of silicon-based intracortical microelectrode arrays in non-human primates. *Journal of Neural Engineering*, 10(6), 2013.
- [16] E. Patrick, M. E. Orazem, J. C. Sanchez, and T. Nishida. Corrosion of tungsten microelectrodes used in neural recording applications. *Journal of Neuroscience Methods*, 198(2):158–171, 2011.
- [17] S. P. Lacour, G. Courtine, and J. Guck. Materials and technologies for soft implantable neuroprostheses. *Nature Reviews Materials*, 1(10), 2016.
- [18] K. C. Spencer, J. C. Sy, K. B. Ramadi, A. M. Graybiel, R. Langer, and M. J. Cima. Characterization of Mechanically Matched Hydrogel Coatings to Improve the Biocompatibility of Neural Implants. *Scientific Reports*, 7(1):1–16, 2017.
- [19] J. C Williams, J. A. Hippensteel, J. Dilgen, W. Shain, and D. R. Kipke. Complex impedance spectroscopy for monitoring tissue responses to inserted neural implants. *Journal of Neural Engineering*, 4(4):410, 2007.
- [20] H. Lee, R. V. Bellamkonda, W. Sun, and M. E. Levenston. Biomechanical analysis of silicon microelectrode-induced strain in the brain. *Journal of Neural Engineering*, 2(4):81–89, 2005.
- [21] J. K. Nguyen, D. J. Park, J. L. Skousen, A. E. Hess-Dunning, D. J. Tyler, S. J. Rowan, C. Weder, and J. R. Capadona. Mechanically-compliant intracortical implants reduce the neuroinflammatory response. *Journal of Neural Engineering*, 11(5):1–27, 2014.
- [22] D. H. Szarowski, M. D. Andersen, S. Retterer, A. J. Spence, M. Isaacson, H. G. Craighead, J. N. Turner, and W. Shain. Brain responses to micro-machined silicon devices. *Brain Research*, 983(1-2):23–35, 2003.
- [23] J. T.W. Kuo, B. J. Kim, S. A. Hara, C. D. Lee, C. A. Gutierrez, T. Q. Hoang, and E. Meng. Novel flexible Parylene neural probe with 3D sheath structure for enhancing tissue integration. *Lab on a Chip*, 13(4):554–561, 2013.
- [24] V. Castagnola, E. Descamps, A. Lecestre, L. Dahan, J. Remaud, L. G. Nowak, and C. Bergaud. Parylene-based flexible neural probes with PEDOT coated surface for brain stimulation and recording. *Biosensors and Bioelectronics*, 67:450–457, 2015.
- [25] C. Hassler, R. P. Von Metzen, P. Ruther, and T. Stieglitz. Characterization of parylene C as an encapsulation material for implanted neural prostheses. *Journal of Biomedical Materials Research - Part B Applied Biomaterials*, 93(1):266–274, 2010.
- [26] A. Lecomte, E. Descamps, and C. Bergaud. A review on mechanical considerations for chronically-implanted neural probes. *Journal of Neural Engineering*, 15(3), 2018.
- [27] M. C. Lo, S. Wang, S. Singh, V. B. Damodaran, I. Ahmed, K. Coffey, D. Barker, K. Saste, K. Kals, H. M. Kaplan, J. Kohn, D. I. Shreiber, and J. D. Zahn. Evaluating

- the in vivo glial response to miniaturized parylene cortical probes coated with an ultra-fast degrading polymer to aid insertion. *Journal of Neural Engineering*, 15(3), 2018.
- [28] K. C. Cheung, P. Renaud, H. Tanila, and K. Djupsund. Flexible polyimide micro-electrode array for in vivo recordings and current source density analysis. *Biosensors and Bioelectronics*, 22(8):1783–1790, 2007.
- [29] M. Jeon, J. Cho, Y. K. Kim, D. Jung, E. S. Yoon, S. Shin, and I. J. Cho. Partially flexible MEMS neural probe composed of polyimide and sucrose gel for reducing brain damage during and after implantation. *Journal of Micromechanics and Microengineering*, 24(2), 2014.
- [30] S. Takeuchi, T. Suzuki, K. Mabuchi, and H. Fujita. 3D flexible multichannel neural probe array. *Journal of Micromechanics and Microengineering*, 14(1):104–107, 2004.
- [31] Dupont Kapton. [www.dupont.com](http://www.dupont.com), 2018.
- [32] H. C. Lee, J. Ejserholm, F. and Gaire, J. Currlin, S. and Schouenborg, L. Wallman, M. Bengtsson, and K. J. Park, K. and Otto. Histological evaluation of flexible neural implants; Flexibility limit for reducing the tissue response? *Journal of Neural Engineering*, 14(3), 2017.
- [33] I. R. Mineev, P. Musienko, A. Hirsch, Q. Barraud, N. Wenger, E. M. Moraud, J. Gandar, M. Capogrosso, T. Milekovic, L. Asboth, R. F. Torres, N. Vachicouras, Q. Liu, N. Pavlova, S. Duis, A. Larmagnac, J. Vörös, S. Micera, Z. Suo, G. Courtine, and S. P. Lacour. Electronic dura mater for long-term multimodal neural interfaces. *Science*, 347(6218):159–163, 2015.
- [34] S. P. Lacour, D. Chan, S. Wagner, T. Li, and Z. Suo. Mechanisms of reversible stretchability of thin metal films on elastomeric substrates. *Applied Physics Letters*, 88(20):1–4, 2006.
- [35] M. Lo, S. Wang, S. Singh, V. B. Damodaran, H. M. Kaplan, J. Kohn, D. I. Shreiber, and J. D. Zahn. Coating flexible probes with an ultra fast degrading polymer to aid in tissue insertion. *Biomedical Microdevices*, 17(2):34, Feb 2015.
- [36] D. Das, Z. Zhang, T. Winkler, M. Mour, C. I. Günter, M. M. Morlock, H. Machens, and A. F. Schilling. *Bioresorption and Degradation of Biomaterials*, pages 317–333. Springer Berlin Heidelberg, Berlin, Heidelberg, 2012.
- [37] R. A. Green and U. G. Hofmann. Organic electrode coatings for next-generation neural interfaces. *Frontiers in Neuroengineering*, 7(May):1–18, 2014.
- [38] D. Kim, J. A. Wiler, D. J. Anderson, D. R. Kipke, and D. C. Martin. Conducting polymers on hydrogel-coated neural electrode provide sensitive neural recordings in auditory cortex. *Acta Biomaterialia*, 6(1):57–62, 2010.
- [39] A. S Hoffman. Hydrogels for biomedical applications. *Advanced Drug Delivery Reviews*, 64:18–23, 2012.
- [40] T. Billiet, M. Vandenhaute, J. Schelfhout, S. V. Vlierberghe, and P. Dubruel. A review of trends and limitations in hydrogel-rapid prototyping for tissue engineering. *Biomaterials*, 33(26):6020–6041, 2012.

- [41] J. Hoffmann, M. Plotner, D. Kuckling, and W. Fischer. Photopatterning of thermally sensitive hydrogels useful for microactuators. *Sensors and Actuators*, 77:139–144, 1999.
- [42] M. Lei, Y. Gu, A. Baldi, R. Siegel, and B. Ziaie. Soft mold-dry etch: a novel hydrogel patterning technique for biomedical applications. *Conference proceedings: Annual International Conference of the IEEE Engineering in Medicine and Biology Society*, 3:1983–6, 02 2004.
- [43] C. Py, P. Reverdy, L. Doppler, J. Bico, B. Roman, and C. N. Baroud. Capillarity induced folding of elastic sheets. *European Physical Journal: Special Topics*, 166(1):67–71, 2009.
- [44] D. H. Kim *et al.* Dissolvable films of silk fibroin for ultrathin conformal bio-integrated electronics. *Nature Materials*, 9(6):1–7, 2010.
- [45] T. Pan, M. Pharr, Y. Ma, R. Ning, Z. Yan, R. Xu, X. Feng, Y. Huang, and J. A. Rogers. Experimental and Theoretical Studies of Serpentine Interconnects on Ultrathin Elastomers for Stretchable Electronics. *Advanced Functional Materials*, 27(37):1–8, 2017.
- [46] Z. Xiang, S. C. Yen, N. Xue, T. Sun, W. M. Tsang, S. Zhang, L. D. Liao, N. V. Thakor, and C. Lee. Ultra-thin flexible polyimide neural probe embedded in a dissolvable maltose-coated microneedle. *Journal of Micromechanics and Microengineering*, 24(6), 2014.
- [47] W. Jensen, K. Yoshida, and U. G. Hofmann. In - Vivo Implant Mechanics of Flexible , Silicon - Based ACREO Microelectrode Arrays in Rat Cerebral Cortex. *IEEE Transactions on Biomedical Engineering*, 53(5):934–940, 2006.
- [48] A. A. Sharp, A. M. Ortega, D. Restrepo, D. Curran-Everett, and K. Gall. In vivo penetration mechanics and mechanical properties of mouse brain tissue at micrometer scales. *IEEE Transactions on Biomedical Engineering*, 56(1):45–53, 2009.
- [49] B. A. Wester, R. H. Lee, and M. C. LaPlaca. Development and characterization of in vivo flexible electrodes compatible with large tissue displacements. *Journal of neural engineering*, 6(2):024002, 2009.
- [50] I. D. Johnston, D. K. McCluskey, C. K.L. Tan, and M. C. Tracey. Mechanical characterization of bulk Sylgard 184 for microfluidics and microengineering. *Journal of Micromechanics and Microengineering*, 24(3), 2014.
- [51] M. Ghosh and K.L. Mittal. *Polyimides: Fundamentals and Applications*. Plastics Engineering. Taylor & Francis, 2009.
- [52] J. D. Kaufman, G. J. Miller, E. F. Morgan, and C. M. Klapperich. Time-dependent mechanical characterization of poly(2-hydroxyethyl methacrylate) hydrogels using nanoindentation and unconfined compression. *Journal of Materials Research*, 23(5):1472–1481, 2008.
- [53] H. Yuk, T. Zhang, G. A. Parada, X. Liu, and X. Zhao. Skin-inspired hydrogel-elastomer hybrids with robust interfaces and functional microstructures. *Nature Communications*, 7(May):1–11, 2016.

- [54] T. Kondo, R. Watanabe, Y. Shimoyama, K. Shinohe, S. A. Kulinich, and S. Iwamori. Effect of reactive oxygen species generated with ultraviolet lamp and plasma on polyimide surface modification. *Surface and Interface Analysis*, 49(11):1069–1077, 2017.
- [55] D. J. Edell, V. V. Toi, V. M. McNeil, and L. D. Clark. Factors Influencing the Biocompatibility of Insertable Silicon Microshafts in Cerebral Cortex. *IEEE Transactions on Biomedical Engineering*, 39(6):635–643, 1992.
- [56] A. Buxboim, K. Rajagopal, A. E.X. Brown, and D. E. Discher. How deeply cells feel: Methods for thin gels. *Journal of Physics Condensed Matter*, 22(19), 2010.
- [57] A. A. Guex, N. Vachicouras, A. E. Hight, M. C. Brown, D. J. Lee, and S. P. Lacour. Conducting polymer electrodes for auditory brainstem implants. *Journal of Materials Chemistry B*, 3(25):5021–5027, 2015.

## Acknowledgements

I would like to thank Prof. Stéphanie Lacour for allowing me to carry out my Master thesis at the Laboratory for Soft Bioelectronic Interfaces, giving me a great opportunity and learning experience. Deepest thanks to my supervisor Dr. Jennifer Macron for her pragmatic advice, for her constant optimism, for guiding me through the steps of the project, helping me when I was in need, but also trusting me to work independently.

A special thank you to Nicolas Vachicouras for involving me in the conformability study and advising me, to Florent-Valéry Coen for all the assistance with cleanroom processes and to Michael Shur, for the suggestions and help setting up the active probes.

My sincerest gratitude to Anthony Guillet (Wyss Center for Bio and Neuroengineering) for helping me overcome issues in the project with useful microfabrication advice.

I would also like to acknowledge the work done by Arnaud Bichat, who performed the rat surgeries.

Finally a very big thank you to the entire LSBI team, for the daily support, for sharing their amazing work and experience with me and making my time in the lab so enjoyable.

The work carried out in this thesis was funded by the ERC–SNSF Backup Scheme Consolidator Grant.